Received: 19 December 2019 | Revised: 20 March 2020 | Accepted: 26 April 2020

DOI: 10.1002/nme.6389

RESEARCH ARTICLE

WILEY

A framework for data-driven structural analysis in general elasticity based on nonlinear optimization: The dynamic case

Cristian Guillermo Gebhardt[1] | **Marc Christian Steinbach**[2] | **Dominik Schillinger**[3] | **Raimund Rolfes**[1]

[1]Institute of Structural Analysis - ForWind Hannover, Leibniz Universität Hannover, Hannover, Germany

[2]Institute of Applied Mathematics, Leibniz Universität Hannover, Hannover, Germany

[3]Institute of Mechanics and Computational Mechanics, Leibniz Universität Hannover, Hannover, Germany

Correspondence
Cristian Guillermo Gebhardt, Institute of Structural Analysis - ForWind Hannover, Leibniz Universität Hannover, Appelstraße 9A, 30167 Hannover, Germany.
Email: c.gebhardt@isd.uni-hannover.de

Funding information
Deutsche Forschungsgemeinschaft, Grant/Award Numbers: "ENERGIZE", GE 2773/3-1 and RO 706/20-1 and Emmy Noether Award, SCH 1249/2-1; European Research Council, Grant/Award Number: "ImageToSim", Action No. 759001; Niedersächsisches Ministerium für Wissenschaft und Kultur, Grant/Award Number: "ventus efficiens", FKZ ZN3024

Summary

In this article, we present an extension of the formulation recently developed by the authors to the structural dynamics setting. Inspired by a structure-preserving family of variational integrators, our new formulation relies on a discrete balance equation that establishes the dynamic equilibrium. From this point of departure, we first derive an "exact" discrete-continuous nonlinear optimization problem that works directly with data sets. We then develop this formulation further into an "approximate" nonlinear optimization problem that relies on a general constitutive model. This underlying model can be identified from a data set in an offline phase. To showcase the advantages of our framework, we specialize our methodology to the case of a geometrically exact beam formulation that makes use of all elements of our approach. We investigate three numerical examples of increasing difficulty that demonstrate the excellent computational behavior of the proposed framework and motivate future research in this direction.

KEYWORDS

data-driven structural dynamics, finite elements, geometrically exact beams, nonlinear optimization problem, structure-preserving time integration

1 | INTRODUCTION

Data-Driven Computational Mechanics is a new computing philosophy that enables the evolution from conventional data-free methods to modern data-rich approaches. Its underlying concept relies on the reformulation of classical boundary value problems of elasticity and inelasticity such that material models, which are calibrated from experiments, are replaced by some form of experimental material data. On the one hand, Data-Driven Computational Mechanics eliminates some modeling errors and the associated uncertainty by employing experimental data directly. On the other hand, new sources of error emerge that are associated with

the measurements and with the particular measuring technology employed. At least for the moment, there is no consensus regarding which sources of error are the most severe, and therefore, there is still a long way to go.

Among recent developments, two principal approaches of Data-Driven Computational Mechanics can be distinguished. On the one hand, there is a *direct* one,[1,2] whose methods are based on a discrete-continuous optimization problem that attempts to assign to each material point a point in the phase space that under fulfillment of the compatibility and equilibrium constraints is closest to the data set provided. Within that framework, some very interesting advances are reported, for instance, regarding nonlinear elasticity,[3] general elasticity,[4] inelasticity,[5] and mixed-integer quadratic optimization problems.[6] On the other hand, there is an *inverse* one,[7-9] whose methods rely on an inverse approach that attempts to reconstruct from the data sets provided a constitutive manifold with a well-defined functional structure. In the context of these two families of methods, our recent work on approximate nonlinear optimization problems[10] represents a *hybrid* approach, targeting at a synergistic compromise that combines their strengths and mitigates some of their main weaknesses, in particular the high computational cost associated with the resolution of a discrete-continuous nonlinear optimization problem for the *direct* approach and the limitation to a special functional structure that only allows the explicit definition of stresses for the *inverse* approach.

Data-Driven Structural Dynamics, the application of Data-Driven Computational Mechanics principles to structural dynamics problems, is currently less developed, with a few papers published so far. For instance, in Reference 11, the data-driven solvers for quasistatic problems developed in References 1,2 were extended to dynamics, relying on variational time-stepping schemes such as the Newmark algorithm. In Reference 12, a thermodynamically consistent approach that relies on the "General Equation for Non-Equilibrium Reversible-Irreversible Coupling" formalism was presented, which enforces by design the conservation of energy and positive production of entropy.

The central goal of the present work is the formulation of an approximate nonlinear optimization problem for Data-Driven Structural Dynamics, which can be understood as the structural dynamics counterpart of the formulation previously developed by the authors in Reference 10. The proposed approximate nonlinear optimization problem relies on a discrete balance equation, which is inspired by a class of variational integrators[13-20] and represents the dynamic equilibrium. Since in our approach, no special functional structure of the constitutive manifold is assumed, the existence of an energy function is in general not guaranteed, and therefore, energy-momentum methods[19,21-24] are not directly applicable. First, the proposed framework improves computational efficiency and robustness with respect to the type of solvers that rely on discrete-continuous optimization problems. In particular, our approximate nonlinear optimization problem can be solved with local sequential quadratic programming methods, circumventing the necessity of employing meta-heuristic methods. Second, the proposed framework can deal with implicitly defined stress-strain relations and kinematic constraints, thus enlarging its range of applicability. Finally, we consider the case of a geometrically exact beam element to demonstrate the advantages of our approach. Such a finite element model makes full use of our computational machinery. Be aware that our primary goal is a proof of concept for our new approximate nonlinear optimization approach for Data-Driven Structural Dynamics, and therefore, the identification of the underlying constitutive manifold is not addressed here.

The remainder of this work is organized as follows: Section 2, the core of this article, presents two optimization problems for Data-Driven Structural Dynamics that are built upon a time integration approach inspired by a class of structure-preserving methods. The first one is an "exact" discrete-continuous nonlinear optimization problem that works directly with data sets. Such a problem can be considered as the starting point and is not going to be solved within this work. The second one is an "approximate" nonlinear optimization problem that relies on a general approximation of the underlying constitutive manifold, which circumvents completely the necessity of online handling of data sets. For both problems, we define the associated Lagrangian functions and derive explicitly the first order optimality conditions as well as the corresponding KKT matrices. We also carefully discuss the differences between the static and dynamic cases. In Section 3, we specialize the proposed methodology for the geometrically exact beam finite element in a purely dynamic setting. This particular structural model has been chosen because it makes use of all elements of our approach. Section 4 presents simulation results that illustrate the capability of the derived approach with special emphasis on preserved quantities along the discrete motion, which is seen as the solution of a sequence of successive nonlinear optimization problems. Finally, in Section 5, we draw concluding remarks and propose future work.

2 | NONLINEAR OPTIMIZATION PROBLEMS

The definition of successive nonlinear optimization problems in Data-Driven Structural Dynamics implies the partitioning of the considered time interval $[t_a, t_b]$ into subintervals $[t_i, t_{i+1}]$ such that $t_a = t_0 < \ldots < t_N = t_b$. We consider an equidistant partitioning by a fixed time step, that is, $t_{i+1} - t_i = \Delta t \; \forall i \in [0, N-1]$. A very simple scalar cost function to be minimized at time instant $t_{i+\frac{1}{2}} \in (t_i, t_{i+1})$ can be defined as

$$\mathcal{J}(\tilde{\boldsymbol{e}}_{i+\frac{1}{2}}, \tilde{\boldsymbol{s}}_{i+\frac{1}{2}}, \boldsymbol{e}_{i+\frac{1}{2}}, \boldsymbol{s}_{i+\frac{1}{2}}) = \frac{1}{2}\|\boldsymbol{e}_{i+\frac{1}{2}} - \tilde{\boldsymbol{e}}_{i+\frac{1}{2}}\|^2_{\boldsymbol{C}} + \frac{1}{2}\|\boldsymbol{s}_{i+\frac{1}{2}} - \tilde{\boldsymbol{s}}_{i+\frac{1}{2}}\|^2_{\boldsymbol{C}^{-1}}, \tag{1}$$

where the pair $(\boldsymbol{e}_{i+\frac{1}{2}}, \boldsymbol{s}_{i+\frac{1}{2}}) \in \mathcal{Z}$ denotes continuous strain and stress variables $\boldsymbol{e}_{i+\frac{1}{2}}$ and $\boldsymbol{s}_{i+\frac{1}{2}}$, respectively, a given finite data set $\tilde{\mathcal{Z}}$ contains strain and stress measurements $(\tilde{\boldsymbol{e}}_{i+\frac{1}{2}}, \tilde{\boldsymbol{s}}_{i+\frac{1}{2}})$, $\boldsymbol{C} \in \mathbb{R}^{n_e \times n_e}$ is a symmetric positive-definite weight matrix with inverse $\boldsymbol{C}^{-1}$, and $\|\cdot\|_{\boldsymbol{C}}$ and $\|\cdot\|^{-1}_{\boldsymbol{C}}$ are norms derived from an inner product. At this point, there is no necessity to specify n_e since it depends on the structural model considered, which for now remains unspecified. The cost function (1) has to be minimized under the following constraints: (i) the compatibility equation that enforces the equivalence between strain variables and displacement-based strains at time instant $t_{i+\frac{1}{2}}$,

$$\boldsymbol{e}_{i+\frac{1}{2}} - \boldsymbol{e}(\boldsymbol{q}_{i+\frac{1}{2}}) = \boldsymbol{0}, \tag{2}$$

in which $\boldsymbol{q}_{i+\frac{1}{2}} \in Q \subset \mathbb{R}^{m+n}$ is the vector of generalized coordinates and Q stands for the configuration manifold; (ii) the discrete balance equation that establishes the dynamic equilibrium, for instance, we chose an approximation inspired by a family of variational integrators[13-20] that renders the dynamic equilibrium at time instant t_i as

$$\boldsymbol{M}\frac{\boldsymbol{q}_{i+1} - 2\boldsymbol{q}_i + \boldsymbol{q}_{i-1}}{\Delta t} + \frac{\Delta t}{2}\left(\boldsymbol{B}(\boldsymbol{q}_{i-\frac{1}{2}})^T\boldsymbol{s}_{i-\frac{1}{2}} + \boldsymbol{B}(\boldsymbol{q}_{i+\frac{1}{2}})^T\boldsymbol{s}_{i+\frac{1}{2}}\right) + \Delta t\boldsymbol{G}(\boldsymbol{q}_i)^T\chi_i - \frac{\Delta t}{2}\left(\boldsymbol{f}^{\text{ext}}_{i-\frac{1}{2}} + \boldsymbol{f}^{\text{ext}}_{i+\frac{1}{2}}\right) = \boldsymbol{0}, \tag{3}$$

in which $\boldsymbol{M} \in T^*_{\boldsymbol{q}}Q \times T^*_{\boldsymbol{q}}Q$ represents the constant mass matrix,

$$\boldsymbol{q}_{i-\frac{1}{2}} \approx \frac{\boldsymbol{q}_{i-1} + \boldsymbol{q}_i}{2} \quad \text{and} \quad \boldsymbol{q}_{i+\frac{1}{2}} \approx \frac{\boldsymbol{q}_i + \boldsymbol{q}_{i+1}}{2}, \tag{4}$$

$\boldsymbol{B}(\boldsymbol{q}_{i+\frac{1}{2}}) = \partial_{\boldsymbol{q}_{i+\frac{1}{2}}}\boldsymbol{e}(\boldsymbol{q}_{i+\frac{1}{2}}) \in L(T_{\boldsymbol{q}_{i+\frac{1}{2}}}Q, \mathbb{R}^{n_e})$ is the Jacobian matrix of the displacement-based strains, similarly for $\boldsymbol{B}(\boldsymbol{q}_{i-\frac{1}{2}})$, $\boldsymbol{G}(\boldsymbol{q}_i) = \partial_{\boldsymbol{q}_i}\boldsymbol{g}(\boldsymbol{q}_i) \in L(T_{\boldsymbol{q}_i}Q, \mathbb{R}^m)$ is the Jacobian matrix of the kinematic constraints at time instant t_i, $\chi_i \in \mathbb{R}^m$ is the corresponding vector of Lagrange multipliers, and $\boldsymbol{f}^{\text{ext}}_{i+\frac{1}{2}} \in T^*_{\boldsymbol{q}_{i+\frac{1}{2}}}Q$ represents the vector of generalized external loads, similarly for $\boldsymbol{f}^{\text{ext}}_{i-\frac{1}{2}}$; and, (iii) the kinematic constraints at time instant t_{i+1},

$$\boldsymbol{g}(\boldsymbol{q}_{i+1}) = \boldsymbol{0}, \tag{5}$$

a finite set of integrable restrictions that belongs to $\mathbb{R}^m$. As usual in the finite element setting, we assume that the Jacobian matrix of the displacement-based strains $\boldsymbol{B}(\boldsymbol{q})$ and the Jacobian matrix of the constraints $\boldsymbol{G}(\boldsymbol{q})$ are linear in $\boldsymbol{q}$, yielding substantial simplifications when calculating higher-order derivatives. Since the existence of an energy function is in general not guaranteed, energy-momentum methods are not directly applicable.[19,21-24]

Now, to briefly investigate the conservation properties of the adopted time integration scheme, let us first neglect the external forces and define the discrete momenta:

$$\boldsymbol{p}^+_i = \boldsymbol{M}\frac{\boldsymbol{q}_i - \boldsymbol{q}_{i-1}}{\Delta t} - \frac{\Delta t}{2}\boldsymbol{B}(\boldsymbol{q}_{i-\frac{1}{2}})^T\boldsymbol{s}_{i-\frac{1}{2}} - \frac{\Delta t}{2}\boldsymbol{G}(\boldsymbol{q}_i)^T\chi_i \in T^*_{\boldsymbol{q}_i}Q, \tag{6a}$$

$$\boldsymbol{p}^-_i = \boldsymbol{M}\frac{\boldsymbol{q}_{i+1} - \boldsymbol{q}_i}{\Delta t} + \frac{\Delta t}{2}\boldsymbol{B}(\boldsymbol{q}_{i+\frac{1}{2}})^T\boldsymbol{s}_{i+\frac{1}{2}} + \frac{\Delta t}{2}\boldsymbol{G}(\boldsymbol{q}_i)^T\chi_i \in T^*_{\boldsymbol{q}_i}Q. \tag{6b}$$

These definitions are inspired by the discrete Legendre transforms that are widely used in the context of variational integrators. Having at hand the discrete momenta, the discrete balance equation can be rewritten as $\boldsymbol{p}^+_i - \boldsymbol{p}^-_i = \boldsymbol{0}$, which

leads to the existence of a unique momentum $\boldsymbol{p}_i$ at time instant t_i. In this discrete setting, there are two possible definitions of linear momentum, namely

$$\boldsymbol{l}_i^- = \sum_{a=1}^{N_{\text{nodes}}} \mathfrak{L}_{\text{trans}}(\boldsymbol{p}_i^-)_a \quad \text{and} \quad \boldsymbol{l}_i^+ = \sum_{a=1}^{N_{\text{nodes}}} \mathfrak{L}_{\text{trans}}(\boldsymbol{p}_i^+)_a, \tag{7}$$

in which $\mathfrak{L}_{\text{trans}}$ filters out all non-translational contributions and N_{nodes} denotes the number of nodes. Provided that the system under consideration is invariant under translations, that is, the orthogonality between the internal forces and the infinitesimal generator of translation is given, a unique discrete linear momentum does exist, namely $\boldsymbol{l}_d(\boldsymbol{q}_i, \boldsymbol{q}_{i+1}) = \boldsymbol{l}_i^- = \boldsymbol{l}_i^+$, and is an invariant of the discrete motion, whose conservation law reads

$$\boldsymbol{l}_d(\boldsymbol{q}_i, \boldsymbol{q}_{i+1}) - \boldsymbol{l}_d(\boldsymbol{q}_{i-1}, \boldsymbol{q}_i) = \boldsymbol{0}. \tag{8}$$

Likewise, there are two possible definitions of angular momentum, namely

$$\boldsymbol{j}_i^- = \sum_{a=1}^{N_{\text{nodes}}} (\boldsymbol{q}_i)_a \times (\boldsymbol{p}_i^-)_a \quad \text{and} \quad \boldsymbol{j}_i^+ = \sum_{a=1}^{N_{\text{nodes}}} (\boldsymbol{q}_{i+1})_a \times (\boldsymbol{p}_i^+)_a. \tag{9}$$

Similarly, provided that the system under consideration is invariant under rotations, that is, the orthogonality between the internal forces and the infinitesimal generator of the rotation is given, a unique discrete angular momentum does exist, namely $\boldsymbol{j}_d(\boldsymbol{q}_i, \boldsymbol{q}_{i+1}) = \boldsymbol{j}_i^- = \boldsymbol{j}_i^+$, and is an invariant of the discrete motion, whose conservation law reads

$$\boldsymbol{j}_d(\boldsymbol{q}_i, \boldsymbol{q}_{i+1}) - \boldsymbol{j}_d(\boldsymbol{q}_{i-1}, \boldsymbol{q}_i) = \boldsymbol{0}. \tag{10}$$

Finally, to avoid problems caused by overdetermination and singular KKT matrices in the subsequent optimization problems, we eliminate the Lagrange multipliers from (3) by means of the null-space method. This requires a null-space basis matrix $\boldsymbol{N}(\boldsymbol{q}_i) \in L(\mathbb{R}^n, T_{\boldsymbol{q}_i}Q)$ for $\ker(\boldsymbol{G}(\boldsymbol{q}_i)) = \{\boldsymbol{n} \in T_{\boldsymbol{q}_i}Q | \boldsymbol{G}(\boldsymbol{q}_i)\boldsymbol{n} = \boldsymbol{0} \in \mathbb{R}^m\}$ with $n = \dim(Q) - m$, the system's number of degrees of freedom, and $\operatorname{rank}(\boldsymbol{N}(\boldsymbol{q}_i)) = \dim(\ker(\boldsymbol{G}(\boldsymbol{q}_i))) = n$, such that

$$\boldsymbol{G}(\boldsymbol{q}_i)\boldsymbol{N}(\boldsymbol{q}_i) = \boldsymbol{0}. \tag{11}$$

Then, dynamic equilibrium adopts the form

$$\boldsymbol{0} = \boldsymbol{N}(\boldsymbol{q}_i)^T \left(\boldsymbol{M}\frac{\boldsymbol{q}_{i+1} - 2\boldsymbol{q}_i + \boldsymbol{q}_{i-1}}{\Delta t} + \frac{\Delta t}{2}\left(\boldsymbol{B}(\boldsymbol{q}_{i-\frac{1}{2}})^T \boldsymbol{s}_{i-\frac{1}{2}} + \boldsymbol{B}(\boldsymbol{q}_{i+\frac{1}{2}})^T \boldsymbol{s}_{i+\frac{1}{2}}\right) - \frac{\Delta t}{2}\left(\boldsymbol{f}^{\text{ext}}_{i-\frac{1}{2}} + \boldsymbol{f}^{\text{ext}}_{i+\frac{1}{2}}\right)\right) \tag{12a}$$

$$= \boldsymbol{f}(\boldsymbol{q}_{i+1}, \boldsymbol{s}_{i+\frac{1}{2}}), \tag{12b}$$

where only the dependency on unknown quantities is explicitly indicated in $\boldsymbol{f}(\boldsymbol{q}_{i+1}, \boldsymbol{s}_{i+\frac{1}{2}})$.

2.1 | The "exact" discrete-continuous nonlinear optimization problem

Definition 1 (Exact DCNLP): Employing directly the strain and stress measurements, each successive "Data-Driven Structural Dynamics" problem can be defined as a discrete-continuous nonlinear optimization problem that can be stated as

$$\min_{(\tilde{\boldsymbol{e}}_{i+\frac{1}{2}}, \tilde{\boldsymbol{s}}_{i+\frac{1}{2}}, \boldsymbol{q}_{i+1}, \boldsymbol{e}_{i+\frac{1}{2}}, \boldsymbol{s}_{i+\frac{1}{2}})} \quad \frac{1}{2}\|\boldsymbol{e}_{i+\frac{1}{2}} - \tilde{\boldsymbol{e}}_{i+\frac{1}{2}}\|_{\boldsymbol{C}}^2 + \frac{1}{2}\|\boldsymbol{s}_{i+\frac{1}{2}} - \tilde{\boldsymbol{s}}_{i+\frac{1}{2}}\|_{\boldsymbol{C}^{-1}}^2$$

$$\text{subject to} \qquad \boldsymbol{e}_{i+\frac{1}{2}} - \boldsymbol{e}(\boldsymbol{q}_{i+\frac{1}{2}}) = \boldsymbol{0},$$

$$\boldsymbol{f}(\boldsymbol{q}_{i+1}, \boldsymbol{s}_{i+\frac{1}{2}}) = \boldsymbol{0},$$

$$\boldsymbol{g}(\boldsymbol{q}_{i+1}) = \boldsymbol{0}. \tag{13}$$

Note that the discrete variables $(\tilde{\boldsymbol{e}}_{i+\frac{1}{2}}, \tilde{\boldsymbol{s}}_{i+\frac{1}{2}}) \in \tilde{\mathcal{Z}}$ at time instant $t_{i+\frac{1}{2}}$ appear only in the cost function. For fixed $(\tilde{\boldsymbol{e}}_{i+\frac{1}{2}}, \tilde{\boldsymbol{s}}_{i+\frac{1}{2}})$, the exact DCNLP becomes a smooth nonlinear optimization problem (NLP), referred to as NLP$(\tilde{\boldsymbol{e}}_{i+\frac{1}{2}}, \tilde{\boldsymbol{s}}_{i+\frac{1}{2}})$. Any solution provides a set of values $(\boldsymbol{q}_{i+1}, \boldsymbol{e}_{i+\frac{1}{2}}, \boldsymbol{s}_{i+\frac{1}{2}})$ that (locally) minimizes the cost function for the fixed data point under the constraints given above.

Theorem 1. *The first-order optimality conditions of* NLP$(\tilde{\boldsymbol{e}}_{i+\frac{1}{2}}, \tilde{\boldsymbol{s}}_{i+\frac{1}{2}})$ *are:*

$$\delta \boldsymbol{q}_{i+1} \,:\, -\frac{1}{2}\boldsymbol{B}(\boldsymbol{q}_{i+\frac{1}{2}})^T \boldsymbol{\lambda}_{i+\frac{1}{2}} + \boldsymbol{F}(\boldsymbol{s}_{i+\frac{1}{2}})^T \boldsymbol{\mu}_i + \boldsymbol{G}(\boldsymbol{q}_{i+1})^T \boldsymbol{\nu}_{i+1} = \boldsymbol{0}, \tag{14a}$$

$$\delta \boldsymbol{e}_{i+\frac{1}{2}} \,:\, \boldsymbol{C}(\boldsymbol{e}_{i+\frac{1}{2}} - \tilde{\boldsymbol{e}}_{i+\frac{1}{2}}) + \boldsymbol{\lambda}_{i+\frac{1}{2}} = \boldsymbol{0}, \tag{14b}$$

$$\delta \boldsymbol{s}_{i+\frac{1}{2}} \,:\, \boldsymbol{C}^{-1}(\boldsymbol{s}_{i+\frac{1}{2}} - \tilde{\boldsymbol{s}}_{i+\frac{1}{2}}) + \frac{\Delta t}{2}\boldsymbol{B}(\boldsymbol{q}_{i+\frac{1}{2}})\boldsymbol{N}(\boldsymbol{q}_i)\boldsymbol{\mu}_i = \boldsymbol{0}, \tag{14c}$$

$$\delta \boldsymbol{\lambda}_{i+\frac{1}{2}} \,:\, \boldsymbol{e}_{i+\frac{1}{2}} - \boldsymbol{e}(\boldsymbol{q}_{i+\frac{1}{2}}) = \boldsymbol{0}, \tag{14d}$$

$$\delta \boldsymbol{\mu}_i \,:\, \boldsymbol{f}(\boldsymbol{q}_{i+1}, \boldsymbol{s}_{i+\frac{1}{2}}) = \boldsymbol{0}, \tag{14e}$$

$$\delta \boldsymbol{\nu}_{i+1} \,:\, \boldsymbol{g}(\boldsymbol{q}_{i+1}) = \boldsymbol{0}, \tag{14f}$$

where we define

$$\boldsymbol{F}(\boldsymbol{s}_{i+\frac{1}{2}}) := \partial_{\boldsymbol{q}_{i+1}} \boldsymbol{f}(\boldsymbol{q}_{i+1}, \boldsymbol{s}_{i+\frac{1}{2}}) = \boldsymbol{N}(\boldsymbol{q}_i)^T \left(\frac{1}{\Delta t}\boldsymbol{M} + \frac{\Delta t}{4}\boldsymbol{U}_2(\boldsymbol{s}_{i+\frac{1}{2}}) \right) \tag{15}$$

with

$$\boldsymbol{U}_2(\boldsymbol{s}) := \partial_{\boldsymbol{q}}(\boldsymbol{B}(\boldsymbol{q})^T \boldsymbol{s}) = \boldsymbol{U}_2(\boldsymbol{s})^T. \tag{16}$$

Proof. The Lagrangian function of NLP$(\tilde{\boldsymbol{e}}_{i+\frac{1}{2}}, \tilde{\boldsymbol{s}}_{i+\frac{1}{2}})$ is

$$\begin{aligned} \mathcal{L}_{\text{fix}}(\boldsymbol{q}_{i+1}, \boldsymbol{e}_{i+\frac{1}{2}}, \boldsymbol{s}_{i+\frac{1}{2}}, \boldsymbol{\lambda}_{i+\frac{1}{2}}, \boldsymbol{\mu}_i, \boldsymbol{\nu}_{i+1}; \tilde{\boldsymbol{e}}_{i+\frac{1}{2}}, \tilde{\boldsymbol{s}}_{i+\frac{1}{2}}) = {} & \frac{1}{2}\|\boldsymbol{e}_{i+\frac{1}{2}} - \tilde{\boldsymbol{e}}_{i+\frac{1}{2}}\|^2_{\boldsymbol{C}} + \frac{1}{2}\|\boldsymbol{s}_{i+\frac{1}{2}} - \tilde{\boldsymbol{s}}_{i+\frac{1}{2}}\|^2_{\boldsymbol{C}^{-1}} \\ & + \boldsymbol{\lambda}^T_{i+\frac{1}{2}} \left(\boldsymbol{e}_{i+\frac{1}{2}} - \boldsymbol{e}(\boldsymbol{q}_{i+\frac{1}{2}}) \right) \\ & + \boldsymbol{\mu}_i{}^T \boldsymbol{f}(\boldsymbol{q}_{i+1}, \boldsymbol{s}_{i+\frac{1}{2}}) \\ & + \boldsymbol{\nu}_{i+1}{}^T \boldsymbol{g}(\boldsymbol{q}_{i+1}), \end{aligned} \tag{17}$$

where $\boldsymbol{\lambda}_{i+\frac{1}{2}} \in \mathbb{R}^{n_e}$ are Lagrange multipliers of the compatibility equation at time instant $t_{i+\frac{1}{2}}$, $\boldsymbol{\mu}_i \in \mathbb{R}^n$ are Lagrange multipliers of the balance equation premultiplied by the null-space basis matrix evaluated at time instant t_i, and $\boldsymbol{\nu}_{i+1} \in \mathbb{R}^m$ are Lagrange multipliers of kinematic constraints at the instant t_{i+1}. To derive the corresponding first-order optimality conditions, we calculate the variation of $\mathcal{L}_{\text{fix}}$ as

$$\delta\mathcal{L}_{\text{fix}}(\boldsymbol{q}_{i+1}, \boldsymbol{e}_{i+\frac{1}{2}}, \boldsymbol{s}_{i+\frac{1}{2}}, \boldsymbol{\lambda}_{i+\frac{1}{2}}, \boldsymbol{\mu}_i, \boldsymbol{\nu}_{i+1}; \tilde{\boldsymbol{e}}_{i+\frac{1}{2}}, \tilde{\boldsymbol{s}}_{i+\frac{1}{2}}) = \partial_{\boldsymbol{x}_{\text{fix}}} \mathcal{L}_{\text{fix}}(\boldsymbol{x}_{\text{fix}}; \tilde{\boldsymbol{e}}_{i+\frac{1}{2}}, \tilde{\boldsymbol{s}}_{i+\frac{1}{2}}) \delta \boldsymbol{x}_{\text{fix}} \tag{18}$$

with the primal-dual NLP variable vector

$$\boldsymbol{x}_{\text{fix}} := (\boldsymbol{q}_{i+1}^T, \boldsymbol{e}_{i+\frac{1}{2}}^T, \boldsymbol{s}_{i+\frac{1}{2}}^T, \lambda_{i+\frac{1}{2}}^T, \boldsymbol{\mu}_i{}^T, \boldsymbol{\nu}_{i+1}{}^T)^T, \tag{19}$$

obtaining

$$\begin{aligned}\partial_{\boldsymbol{x}_{\text{fix}}}\mathcal{L}_{\text{fix}}(\boldsymbol{x}_{\text{fix}};\tilde{\boldsymbol{e}}_{i+\frac{1}{2}},\tilde{\boldsymbol{s}}_{i+\frac{1}{2}})\delta\boldsymbol{x}_{\text{fix}} = {}& \delta\boldsymbol{q}_{i+1}^T\left(-\frac{1}{2}\boldsymbol{B}(\boldsymbol{q}_{i+\frac{1}{2}})^T\lambda_{i+\frac{1}{2}} + \left(\partial_{\boldsymbol{q}_{i+1}}\boldsymbol{f}(\boldsymbol{q}_{i+1},\boldsymbol{s}_{i+\frac{1}{2}})\right)^T\boldsymbol{\mu}_i + \boldsymbol{G}(\boldsymbol{q}_{i+1})^T\boldsymbol{\nu}_{i+1}\right)\\ &+ \delta\boldsymbol{e}_{i+\frac{1}{2}}^T\left(\boldsymbol{C}(\boldsymbol{e}_{i+\frac{1}{2}} - \tilde{\boldsymbol{e}}_{i+\frac{1}{2}}) + \lambda_{i+\frac{1}{2}}\right)\\ &+ \delta\boldsymbol{s}_{i+\frac{1}{2}}^T\left(\boldsymbol{C}^{-1}(\boldsymbol{s}_{i+\frac{1}{2}} - \tilde{\boldsymbol{s}}_{i+\frac{1}{2}}) + \frac{\Delta t}{2}\boldsymbol{B}(\boldsymbol{q}_{i+\frac{1}{2}})\boldsymbol{N}(\boldsymbol{q}_i)\boldsymbol{\mu}_i\right)\\ &+ \delta\lambda_{i+\frac{1}{2}}^T\left(\boldsymbol{e}_{i+\frac{1}{2}} - \boldsymbol{e}(\boldsymbol{q}_{i+\frac{1}{2}})\right)\\ &+ \delta\boldsymbol{\mu}_i{}^T\boldsymbol{f}(\boldsymbol{q}_{i+1},\boldsymbol{s}_{i+\frac{1}{2}})\\ &+ \delta\boldsymbol{\nu}_{i+1}{}^T\boldsymbol{g}(\boldsymbol{q}_{i+1}).\end{aligned} \tag{20}$$

Setting this to zero for any choice of the varied quantities yields the KKT conditions (14). ■

Note that $\boldsymbol{e}_{i+\frac{1}{2}}$ and $\lambda_{i+\frac{1}{2}}$ can be eliminated by substitution, but as we are interested in the problem's global format, we are not going to eliminate anything unless strictly necessary.

The linearization of the variation of $\mathcal{L}_{\text{fix}}$ reads

$$\Delta\delta\mathcal{L}_{\text{fix}}(\boldsymbol{x}_{\text{fix}};\tilde{\boldsymbol{e}}_{i+\frac{1}{2}},\tilde{\boldsymbol{s}}_{i+\frac{1}{2}}) = \delta\boldsymbol{x}_{\text{fix}}^T\boldsymbol{S}_{\text{fix}}(\boldsymbol{q}_{i+1},\boldsymbol{s}_{i+\frac{1}{2}},\lambda_{i+\frac{1}{2}},\boldsymbol{\mu}_i,\boldsymbol{\nu}_{i+1})\Delta\boldsymbol{x}_{\text{fix}}, \tag{21}$$

where the KKT matrix $\boldsymbol{S}_{\text{fix}}$ is symmetric indefinite and can be written

$$\boldsymbol{S}_{\text{fix}}(\boldsymbol{q}_{i+1},\boldsymbol{s}_{i+\frac{1}{2}},\lambda_{i+\frac{1}{2}},\boldsymbol{\mu}_i,\boldsymbol{\nu}_{i+1}) =$$

$$\begin{bmatrix} -\frac{1}{4}\boldsymbol{U}_2(\lambda_{i+\frac{1}{2}}) + \boldsymbol{V}(\boldsymbol{\nu}_{i+1}) & \boldsymbol{0} & \frac{\Delta t}{4}\boldsymbol{U}_1(\boldsymbol{N}(\boldsymbol{q}_i)\boldsymbol{\mu}_i)^T & -\frac{1}{2}\boldsymbol{B}(\boldsymbol{q}_{i+\frac{1}{2}})^T & \boldsymbol{F}(\boldsymbol{s}_{i+\frac{1}{2}})^T & \boldsymbol{G}(\boldsymbol{q}_{i+1})^T \\ \boldsymbol{0} & \boldsymbol{C} & \boldsymbol{0} & \boldsymbol{I} & \boldsymbol{0} & \boldsymbol{0} \\ \frac{\Delta t}{4}\boldsymbol{U}_1(\boldsymbol{N}(\boldsymbol{q}_i)\boldsymbol{\mu}_i) & \boldsymbol{0} & \boldsymbol{C}^{-1} & \boldsymbol{0} & \frac{\Delta t}{2}\boldsymbol{B}(\boldsymbol{q}_{i+\frac{1}{2}})\boldsymbol{N}(\boldsymbol{q}_i) & \boldsymbol{0} \\ -\frac{1}{2}\boldsymbol{B}(\boldsymbol{q}_{i+\frac{1}{2}}) & \boldsymbol{I} & \boldsymbol{0} & \boldsymbol{0} & \boldsymbol{0} & \boldsymbol{0} \\ \boldsymbol{F}(\boldsymbol{s}_{i+\frac{1}{2}}) & \boldsymbol{0} & \frac{\Delta t}{2}\boldsymbol{N}(\boldsymbol{q}_i)^T\boldsymbol{B}(\boldsymbol{q}_{i+\frac{1}{2}})^T & \boldsymbol{0} & \boldsymbol{0} & \boldsymbol{0} \\ \boldsymbol{G}(\boldsymbol{q}_{i+1}) & \boldsymbol{0} & \boldsymbol{0} & \boldsymbol{0} & \boldsymbol{0} & \boldsymbol{0} \end{bmatrix}, \tag{22}$$

with

$$\boldsymbol{V}(\boldsymbol{\nu}) := \partial_{\boldsymbol{q}}(\boldsymbol{G}(\boldsymbol{q})^T\boldsymbol{\nu}) = \boldsymbol{V}(\boldsymbol{\nu})^T \quad \text{and} \quad \boldsymbol{U}_1(\boldsymbol{a}) := \partial_{\boldsymbol{q}}(\boldsymbol{B}(\boldsymbol{q})\boldsymbol{a}), \tag{23}$$

for any constant vector $\boldsymbol{a} \in \mathbb{R}^{n+m}$. As the KKT matrix $\boldsymbol{S}_{\text{fix}}$ is non-singular, all local minima are strict minima and NLP$(\tilde{\boldsymbol{e}}_{i+\frac{1}{2}},\tilde{\boldsymbol{s}}_{i+\frac{1}{2}})$ can be solved by local sequential quadratic programming methods.

The overall DCNLP can be treated by meta-heuristic methods. Since it has no useful structure with respect to the discrete variables $(\tilde{\boldsymbol{e}}_{i+\frac{1}{2}},\tilde{\boldsymbol{s}}_{i+\frac{1}{2}}) \in \tilde{\mathcal{Z}}$, a mathematically rigorous solution requires enumeration, that is, finding the minimal value over all measurements $(\tilde{\boldsymbol{e}}_{i+\frac{1}{2}},\tilde{\boldsymbol{s}}_{i+\frac{1}{2}}) \in \tilde{\mathcal{Z}}$ by solving every NLP$(\tilde{\boldsymbol{e}}_{i+\frac{1}{2}},\tilde{\boldsymbol{s}}_{i+\frac{1}{2}})$ globally. Therefore we suggest a different approach: we propose to add suitable structure that enables us to replace the DCNLP with a single approximating NLP, as already done in the static case.[10]

The proposed exact DCNLP for Data-Driven Structural Dynamics can be understood as a further development of the seminal work by Kirchdoerfer and Ortiz.[1,2,11] There are, nevertheless, some important novel contributions of our current work with respect to the state of the art that ought to be clearly stated. The first one is that our approach is capable of dealing with fully nonlinear kinematics and strain measures independently of the structural elements chosen. The second one is that our methodology can naturally handle algebraic constraints, which can be employed for enforcing a particular kinematics based on the unit sphere S^2, the special orthogonal group $SO(3)$, and/or the special Euclidean group $SE(3)$, but can be also employed for enforcing special constitutive restrictions, for example, implicit stress-strain definitions. The third one is that our approach relies on a discrete version of the dynamic equilibrium inspired by a structure-preserving family of variational integrators. Therefore our approach goes beyond what has been already done. On this basis, we derive next an approximate NLP with which we move forward in the remainder of this work.

2.2 | The "approximate" nonlinear optimization problem

The idea here is to replace the measurement data set $\tilde{\mathcal{Z}}$ by enforcing the state to belong to a reconstructed constitutive manifold that has a precise mathematical structure and that is derived from the data set. The underlying assumption is, of course, that such a constitutive manifold exists and that we can reconstruct a (smooth) implicit representation $\boldsymbol{h}$. The reconstructed constitutive manifold (an approximation) will enormously facilitate the task of the data-driven solver, avoiding the cost of solving a DCNLP, either by enumeration, or by heuristic or meta-heuristic methods which can in general only provide approximate solutions that strongly depend on the initial guess and whose convergence properties are inferior when compared to gradient-based methods.

Definition 2. An "approximate" constitutive manifold is defined as

$$\check{\mathcal{Z}} := \{(\check{\boldsymbol{e}}_{i+\frac{1}{2}}, \check{\boldsymbol{s}}_{i+\frac{1}{2}}) \in \mathbb{R}^{2n_e} | \boldsymbol{h}(\check{\boldsymbol{e}}_{i+\frac{1}{2}}, \check{\boldsymbol{s}}_{i+\frac{1}{2}}) = \boldsymbol{0} \in \mathbb{R}^{n_e}\}. \tag{24}$$

It satisfies

$$\|\boldsymbol{h}(\tilde{\boldsymbol{e}}_{i+\frac{1}{2}}, \tilde{\boldsymbol{s}}_{i+\frac{1}{2}})\| \leq \varepsilon \quad \forall\, (\tilde{\boldsymbol{e}}_{i+\frac{1}{2}}, \tilde{\boldsymbol{s}}_{i+\frac{1}{2}}) \in \tilde{\mathcal{Z}}, \tag{25}$$

for some accuracy $\varepsilon > 0$. Additionally, physical consistency requires that $\boldsymbol{h}(\check{\boldsymbol{e}}_{i+\frac{1}{2}}, \boldsymbol{0}) = \boldsymbol{0}$ implies $\check{\boldsymbol{e}}_{i+\frac{1}{2}} = \boldsymbol{0}$ and $\boldsymbol{h}(\boldsymbol{0}, \check{\boldsymbol{s}}_{i+\frac{1}{2}}) = \boldsymbol{0}$ implies $\check{\boldsymbol{s}}_{i+\frac{1}{2}} = \boldsymbol{0}$.

A constitutive manifold is said to be thermomechanically consistent if it is derived from an energy function Ψ such that the following functional structure holds:[7,10,25]

$$\boldsymbol{h}(\check{\boldsymbol{e}}_{i+\frac{1}{2}}, \check{\boldsymbol{s}}_{i+\frac{1}{2}}) = \check{\boldsymbol{s}}_{i+\frac{1}{2}} - \partial_{\check{\boldsymbol{e}}_{i+\frac{1}{2}}} \Psi(\check{\boldsymbol{e}}_{i+\frac{1}{2}}). \tag{26}$$

However, in the case of new composite materials or metamaterials that exhibit nonconvex responses, the reconstruction of the energy function may not be very convenient. More importantly, in some cases, the formulation of an energy function may not even be possible. Thus, we adopt the constitutive manifold $\check{\mathcal{Z}}$ as introduced previously without assuming any special functional structure of the constitutive constraint $\boldsymbol{h}$. Further specializations are possible and should be instantiated for specific applications of the proposed formulation.

Definition 3 (Approximate NLP): Each successive "Data-Driven Structural Dynamics" problem can be approximated as a nonlinear optimization problem of the form

$$\min_{(\check{\boldsymbol{e}}_{i+\frac{1}{2}}, \check{\boldsymbol{s}}_{i+\frac{1}{2}}, \boldsymbol{q}_{i+1}, \boldsymbol{e}_{i+\frac{1}{2}}, \boldsymbol{s}_{i+\frac{1}{2}})} \quad \frac{1}{2}\|\boldsymbol{e}_{i+\frac{1}{2}} - \check{\boldsymbol{e}}_{i+\frac{1}{2}}\|^2_{\boldsymbol{C}} + \frac{1}{2}\|\boldsymbol{s}_{i+\frac{1}{2}} - \check{\boldsymbol{s}}_{i+\frac{1}{2}}\|^2_{\boldsymbol{C}^{-1}}$$

$$\text{subject to} \qquad \boldsymbol{e}_{i+\frac{1}{2}} - \boldsymbol{e}(\boldsymbol{q}_{i+\frac{1}{2}}) = \boldsymbol{0},$$

$$\boldsymbol{f}(\boldsymbol{q}_{i+1}, \boldsymbol{s}_{i+\frac{1}{2}}) = \boldsymbol{0},$$

$$\boldsymbol{g}(\boldsymbol{q}_{i+1}) = \boldsymbol{0},$$

$$\boldsymbol{h}(\check{\boldsymbol{e}}_{i+\frac{1}{2}}, \check{\boldsymbol{s}}_{i+\frac{1}{2}}) = \boldsymbol{0}. \tag{27}$$

Theorem 2. *The first-order optimality conditions of the approximate NLP are:*

$$\delta\check{\boldsymbol{e}}_{i+\frac{1}{2}} \,:\, -\boldsymbol{C}(\boldsymbol{e}_{i+\frac{1}{2}} - \check{\boldsymbol{e}}_{i+\frac{1}{2}}) + \left(\partial_{\check{\boldsymbol{e}}_{i+\frac{1}{2}}} \boldsymbol{h}(\check{\boldsymbol{e}}_{i+\frac{1}{2}}, \check{\boldsymbol{s}}_{i+\frac{1}{2}})\right)^T \boldsymbol{\xi}_{i+\frac{1}{2}} = \boldsymbol{0},$$

$$\delta\check{\boldsymbol{s}}_{i+\frac{1}{2}} \,:\, -\boldsymbol{C}^{-1}(\boldsymbol{s}_{i+\frac{1}{2}} - \check{\boldsymbol{s}}_{i+\frac{1}{2}}) + \left(\partial_{\check{\boldsymbol{s}}_{i+\frac{1}{2}}} \boldsymbol{h}(\check{\boldsymbol{e}}_{i+\frac{1}{2}}, \check{\boldsymbol{s}}_{i+\frac{1}{2}})\right)^T \boldsymbol{\xi}_{i+\frac{1}{2}} = \boldsymbol{0},$$

$$\delta\boldsymbol{q}_{i+1} \,:\, -\frac{1}{2}\boldsymbol{B}(\boldsymbol{q}_{i+\frac{1}{2}})^T\boldsymbol{\lambda}_{i+\frac{1}{2}} + \boldsymbol{F}(\boldsymbol{s}_{i+\frac{1}{2}})^T\boldsymbol{\mu}_i + \boldsymbol{G}(\boldsymbol{q}_{i+1})^T\boldsymbol{\nu}_{i+1} = \boldsymbol{0},$$

$$\delta\boldsymbol{e}_{i+\frac{1}{2}} \,:\, \boldsymbol{C}(\boldsymbol{e}_{i+\frac{1}{2}} - \tilde{\boldsymbol{e}}_{i+\frac{1}{2}}) + \boldsymbol{\lambda}_{i+\frac{1}{2}} = \boldsymbol{0},$$

$$\delta\boldsymbol{s}_{i+\frac{1}{2}} \,:\, \boldsymbol{C}^{-1}(\boldsymbol{s}_{i+\frac{1}{2}} - \tilde{\boldsymbol{s}}_{i+\frac{1}{2}}) + \frac{\Delta t}{2}\boldsymbol{B}(\boldsymbol{q}_{i+\frac{1}{2}})\boldsymbol{N}(\boldsymbol{q}_i)\boldsymbol{\mu}_i = \boldsymbol{0},$$

$$\delta\boldsymbol{\lambda}_{i+\frac{1}{2}} \,:\, \boldsymbol{e}_{i+\frac{1}{2}} - \boldsymbol{e}(\boldsymbol{q}_{i+\frac{1}{2}}) = \boldsymbol{0},$$

$$\delta\boldsymbol{\mu}_i \,:\, \boldsymbol{f}(\boldsymbol{q}_{i+1}, \boldsymbol{s}_{i+\frac{1}{2}}) = \boldsymbol{0},$$

$$\delta\boldsymbol{\nu}_{i+1} \,:\, \boldsymbol{g}(\boldsymbol{q}_{i+1}) = \boldsymbol{0},$$

$$\delta\boldsymbol{\xi}_{i+\frac{1}{2}} \,:\, \boldsymbol{h}(\check{\boldsymbol{e}}_{i+\frac{1}{2}}, \check{\boldsymbol{s}}_{i+\frac{1}{2}}) = \boldsymbol{0}. \tag{28a}$$

Proof. The Lagrangian function of the approximate NLP is given by

$$\begin{aligned}
\mathcal{L}(\check{\boldsymbol{e}}_{i+\frac{1}{2}}, \check{\boldsymbol{s}}_{i+\frac{1}{2}}, \boldsymbol{q}_{i+1}, \boldsymbol{e}_{i+\frac{1}{2}}, \boldsymbol{s}_{i+\frac{1}{2}}, \boldsymbol{\lambda}_{i+\frac{1}{2}}, \boldsymbol{\mu}_i, \boldsymbol{\nu}_{i+1}, \boldsymbol{\xi}_{i+\frac{1}{2}}) &= \mathcal{L}_{\text{fix}}(\boldsymbol{x}_{\text{fix}}; \check{\boldsymbol{e}}_{i+\frac{1}{2}}, \check{\boldsymbol{s}}_{i+\frac{1}{2}}) + \boldsymbol{\xi}_{i+\frac{1}{2}}^T \boldsymbol{h}(\check{\boldsymbol{e}}_{i+\frac{1}{2}}, \check{\boldsymbol{s}}_{i+\frac{1}{2}}) \\
&= \frac{1}{2}\|\boldsymbol{e}_{i+\frac{1}{2}} - \check{\boldsymbol{e}}_{i+\frac{1}{2}}\|_{\boldsymbol{C}}^2 + \frac{1}{2}\|\boldsymbol{s}_{i+\frac{1}{2}} - \check{\boldsymbol{s}}_{i+\frac{1}{2}}\|_{\boldsymbol{C}^{-1}}^2 \\
&\quad + \boldsymbol{\lambda}_{i+\frac{1}{2}}^T \left(\boldsymbol{e}_{i+\frac{1}{2}} - \boldsymbol{e}(\boldsymbol{q}_{i+\frac{1}{2}})\right) \\
&\quad + \boldsymbol{\mu}_i{}^T \boldsymbol{f}(\boldsymbol{q}_{i+1}, \boldsymbol{s}_{i+\frac{1}{2}}) \\
&\quad + \boldsymbol{\nu}_{i+1}{}^T \boldsymbol{g}(\boldsymbol{q}_{i+1}) \\
&\quad + \boldsymbol{\xi}_{i+\frac{1}{2}}^T \boldsymbol{h}(\check{\boldsymbol{e}}_{i+\frac{1}{2}}, \check{\boldsymbol{s}}_{i+\frac{1}{2}}),
\end{aligned} \tag{29}$$

where $\boldsymbol{\xi}_{i+\frac{1}{2}} \in \mathbb{R}^{n_e}$ are Lagrange multipliers that correspond to the enforcement of the strain and stress states to remain on the constitutive manifold.

To find the first-order optimality conditions, the variation of $\mathcal{L}$ is calculated as

$$\partial_{\boldsymbol{x}}\mathcal{L}(\boldsymbol{x})\delta\boldsymbol{x} = \delta\check{\boldsymbol{e}}_{i+\frac{1}{2}}^T \left(\boldsymbol{C}(\check{\boldsymbol{e}}_{i+\frac{1}{2}} - \boldsymbol{e}_{i+\frac{1}{2}}) + \left(\partial_{\check{\boldsymbol{e}}_{i+\frac{1}{2}}} \boldsymbol{h}(\check{\boldsymbol{e}}_{i+\frac{1}{2}}, \check{\boldsymbol{s}}_{i+\frac{1}{2}})\right)^T \boldsymbol{\xi}_{i+\frac{1}{2}}\right)$$

$$+ \delta\check{\boldsymbol{s}}_{i+\frac{1}{2}}^T \left(\boldsymbol{C}^{-1}(\check{\boldsymbol{s}}_{i+\frac{1}{2}} - \boldsymbol{s}_{i+\frac{1}{2}}) + \left(\partial_{\check{\boldsymbol{s}}_{i+\frac{1}{2}}} \boldsymbol{h}(\check{\boldsymbol{e}}_{i+\frac{1}{2}}, \check{\boldsymbol{s}}_{i+\frac{1}{2}})\right)^T \boldsymbol{\xi}_{i+\frac{1}{2}}\right)$$

$$
\begin{aligned}
&+ \delta \boldsymbol{q}_{i+1}^T \left(-\frac{1}{2} \boldsymbol{B}(\boldsymbol{q}_{i+\frac{1}{2}})^T \boldsymbol{\lambda}_{i+\frac{1}{2}} + \boldsymbol{F}(\boldsymbol{s}_{i+\frac{1}{2}})^T \boldsymbol{\mu}_i + \boldsymbol{G}(\boldsymbol{q}_{i+1})^T \boldsymbol{\nu}_{i+1} \right) \\
&+ \delta \boldsymbol{e}_{i+\frac{1}{2}}^T \left(\boldsymbol{C}(\boldsymbol{e}_{i+\frac{1}{2}} - \tilde{\boldsymbol{e}}_{i+\frac{1}{2}}) + \boldsymbol{\lambda}_{i+\frac{1}{2}} \right) \\
&+ \delta \boldsymbol{s}_{i+\frac{1}{2}}^T \left(\boldsymbol{C}^{-1}(\boldsymbol{s}_{i+\frac{1}{2}} - \tilde{\boldsymbol{s}}_{i+\frac{1}{2}}) + \frac{\Delta t}{2} \boldsymbol{B}(\boldsymbol{q}_{i+\frac{1}{2}}) \boldsymbol{N}(\boldsymbol{q}_i) \boldsymbol{\mu}_i \right) \\
&+ \delta \boldsymbol{\lambda}_{i+\frac{1}{2}}^T \left(\boldsymbol{e}_{i+\frac{1}{2}} - \boldsymbol{e}(\boldsymbol{q}_{i+\frac{1}{2}}) \right) \\
&+ \delta \boldsymbol{\mu}_i{}^T \boldsymbol{f}(\boldsymbol{q}_{i+1}, \boldsymbol{s}_{i+\frac{1}{2}}) \\
&+ \delta \boldsymbol{\nu}_{i+1}{}^T \boldsymbol{g}(\boldsymbol{q}_{i+1}) \\
&+ \delta \boldsymbol{\xi}_{i+\frac{1}{2}}^T \boldsymbol{h}(\check{\boldsymbol{e}}_{i+\frac{1}{2}}, \check{\boldsymbol{s}}_{i+\frac{1}{2}}),
\end{aligned} \tag{30}
$$

with

$$
\boldsymbol{x} := (\check{\boldsymbol{e}}_{i+\frac{1}{2}}^T, \check{\boldsymbol{s}}_{i+\frac{1}{2}}^T, \boldsymbol{x}_{\text{fix}}^T, \boldsymbol{\xi}_{i+\frac{1}{2}}^T)^T. \tag{31}
$$

Setting this to zero for any choice of the varied quantities yields the KKT conditions (28). ■

The linearization of the variation of $\mathcal{L}$ can be expressed as

$$
\Delta \delta \mathcal{L}(\boldsymbol{x}) = \delta \boldsymbol{x}^T \boldsymbol{S}(\check{\boldsymbol{e}}_{i+\frac{1}{2}}, \check{\boldsymbol{s}}_{i+\frac{1}{2}}, \boldsymbol{q}_{i+1}, \boldsymbol{s}_{i+\frac{1}{2}}, \boldsymbol{\lambda}_{i+\frac{1}{2}}, \boldsymbol{\mu}_i, \boldsymbol{\nu}_{i+1}, \boldsymbol{\xi}_{i+\frac{1}{2}}) \Delta \boldsymbol{x}. \tag{32}
$$

Here the KKT matrix $\boldsymbol{S}$ can be written as

$$
\boldsymbol{S}(\check{\boldsymbol{e}}_{i+\frac{1}{2}}, \check{\boldsymbol{s}}_{i+\frac{1}{2}}, \boldsymbol{q}_{i+1}, \boldsymbol{s}_{i+\frac{1}{2}}, \boldsymbol{\lambda}_{i+\frac{1}{2}}, \boldsymbol{\mu}_i, \boldsymbol{\nu}_{i+1}, \boldsymbol{\xi}_{i+\frac{1}{2}}) =
$$

$$
\begin{bmatrix}
\boldsymbol{S}_{\check{\boldsymbol{e}}\check{\boldsymbol{e}}}(\check{\boldsymbol{e}}_{i+\frac{1}{2}}, \check{\boldsymbol{s}}_{i+\frac{1}{2}}, \boldsymbol{\xi}_{i+\frac{1}{2}}) & \boldsymbol{S}_{\check{\boldsymbol{s}}\check{\boldsymbol{e}}}(\check{\boldsymbol{e}}_{i+\frac{1}{2}}, \check{\boldsymbol{s}}_{i+\frac{1}{2}}, \boldsymbol{\xi}_{i+\frac{1}{2}})^T & \boldsymbol{S}_{\boldsymbol{x}\check{\boldsymbol{e}}}^T & \partial_{\check{\boldsymbol{e}}_{i+\frac{1}{2}}} \boldsymbol{g}(\check{\boldsymbol{e}}_{i+\frac{1}{2}}, \check{\boldsymbol{s}}_{i+\frac{1}{2}})^T \\
\boldsymbol{S}_{\check{\boldsymbol{s}}\check{\boldsymbol{e}}}(\check{\boldsymbol{e}}_{i+\frac{1}{2}}, \check{\boldsymbol{s}}_{i+\frac{1}{2}}, \boldsymbol{\xi}_{i+\frac{1}{2}}) & \boldsymbol{S}_{\check{\boldsymbol{s}}\check{\boldsymbol{s}}}(\check{\boldsymbol{e}}_{i+\frac{1}{2}}, \check{\boldsymbol{s}}_{i+\frac{1}{2}}, \boldsymbol{\xi}_{i+\frac{1}{2}}) & \boldsymbol{S}_{\boldsymbol{x}_{\text{fix}}\check{\boldsymbol{s}}}^T & \partial_{\check{\boldsymbol{s}}_{i+\frac{1}{2}}} \boldsymbol{g}(\check{\boldsymbol{e}}_{i+\frac{1}{2}}, \check{\boldsymbol{s}}_{i+\frac{1}{2}})^T \\
\boldsymbol{S}_{\boldsymbol{x}_{\text{fix}}\check{\boldsymbol{e}}} & \boldsymbol{S}_{\boldsymbol{x}_{\text{fix}}\check{\boldsymbol{s}}} & \boldsymbol{S}_{\text{fix}}(\boldsymbol{q}_{i+1}, \boldsymbol{s}_{i+\frac{1}{2}}, \boldsymbol{\lambda}_{i+\frac{1}{2}}, \boldsymbol{\mu}_i, \boldsymbol{\nu}_{i+1}) & \boldsymbol{0} \\
\partial_{\check{\boldsymbol{e}}_{i+\frac{1}{2}}} \boldsymbol{g}(\check{\boldsymbol{e}}_{i+\frac{1}{2}}, \check{\boldsymbol{s}}_{i+\frac{1}{2}}) & \partial_{\check{\boldsymbol{s}}_{i+\frac{1}{2}}} \boldsymbol{g}(\check{\boldsymbol{e}}_{i+\frac{1}{2}}, \check{\boldsymbol{s}}_{i+\frac{1}{2}}) & \boldsymbol{0} & \boldsymbol{0}
\end{bmatrix}, \tag{33}
$$

with

$$
\boldsymbol{S}_{\check{\boldsymbol{e}}\check{\boldsymbol{e}}}(\check{\boldsymbol{e}}_{i+\frac{1}{2}}, \check{\boldsymbol{s}}_{i+\frac{1}{2}}, \boldsymbol{\xi}_{i+\frac{1}{2}}) := \boldsymbol{C} + \partial_{\check{\boldsymbol{e}}_{i+\frac{1}{2}}} \left(\partial_{\check{\boldsymbol{e}}_{i+\frac{1}{2}}} \boldsymbol{g}(\check{\boldsymbol{e}}_{i+\frac{1}{2}}, \check{\boldsymbol{s}}_{i+\frac{1}{2}})^T \boldsymbol{\xi}_{i+\frac{1}{2}} \right) = \boldsymbol{S}_{\check{\boldsymbol{e}}\check{\boldsymbol{e}}}(\check{\boldsymbol{e}}_{i+\frac{1}{2}}, \check{\boldsymbol{s}}_{i+\frac{1}{2}}, \boldsymbol{\xi}_{i+\frac{1}{2}})^T, \tag{34a}
$$

$$
\boldsymbol{S}_{\check{\boldsymbol{s}}\check{\boldsymbol{e}}}(\check{\boldsymbol{e}}_{i+\frac{1}{2}}, \check{\boldsymbol{s}}_{i+\frac{1}{2}}, \boldsymbol{\xi}_{i+\frac{1}{2}}) := \partial_{\check{\boldsymbol{s}}_{i+\frac{1}{2}}} \left(\partial_{\check{\boldsymbol{e}}_{i+\frac{1}{2}}} \boldsymbol{g}(\check{\boldsymbol{e}}_{i+\frac{1}{2}}, \check{\boldsymbol{s}}_{i+\frac{1}{2}})^T \boldsymbol{\xi}_{i+\frac{1}{2}} \right), \tag{34b}
$$

$$
\boldsymbol{S}_{\check{\boldsymbol{s}}\check{\boldsymbol{s}}}(\check{\boldsymbol{e}}_{i+\frac{1}{2}}, \check{\boldsymbol{s}}_{i+\frac{1}{2}}, \boldsymbol{\xi}_{i+\frac{1}{2}}) := \boldsymbol{C}^{-1} + \partial_{\check{\boldsymbol{s}}_{i+\frac{1}{2}}} \left(\partial_{\check{\boldsymbol{s}}_{i+\frac{1}{2}}} \boldsymbol{g}(\check{\boldsymbol{e}}_{i+\frac{1}{2}}, \check{\boldsymbol{s}}_{i+\frac{1}{2}})^T \boldsymbol{\xi}_{i+\frac{1}{2}} \right) = \boldsymbol{S}_{\check{\boldsymbol{s}}\check{\boldsymbol{s}}}(\check{\boldsymbol{e}}_{i+\frac{1}{2}}, \check{\boldsymbol{s}}_{i+\frac{1}{2}}, \boldsymbol{\xi}_{i+\frac{1}{2}})^T, \tag{34c}
$$

$$
\boldsymbol{S}_{\boldsymbol{x}_{\text{fix}}\check{\boldsymbol{e}}} := \begin{bmatrix} \boldsymbol{0} & -\boldsymbol{C} & \boldsymbol{0} & \boldsymbol{0} & \boldsymbol{0} \end{bmatrix}^T, \tag{34d}
$$

$$\boldsymbol{S}_{\boldsymbol{x}_{\text{fix}^{\check{\boldsymbol{s}}}}} := \begin{bmatrix} \boldsymbol{0} & \boldsymbol{0} & -\boldsymbol{C}^{-1} & \boldsymbol{0} & \boldsymbol{0} \end{bmatrix}^T. \tag{34e}$$

Again the KKT matrix $\boldsymbol{S}$ is nonsingular, hence all local minima are strict and the approximate NLP is well solvable.

Since the proposed approach is built upon a generic, but sufficiently smooth, identified/reconstructed constitutive manifold, experimental data have no direct influence on the convergence and precision properties of the algorithm employed to solve the approximate NLP. The smoothness requirements on the identified/reconstructed constitutive manifold are those prescribed by the smooth finite-dimensional nonlinear optimization theory. Experimental data have, nevertheless, a direct influence on the offline identification/reconstruction step. The identification/reconstruction from experimental data can be, for instance, carried out by means of manifold learning techniques. It entails the appraisal of the inherent dimension and the shape, in an implicit embedding form, of the low-dimensional intrinsic manifold. Such an underlying manifold is to be described by an atlas of local charts that warrant the required continuity conditions. Moreover, strain-stress representations may become indeed very difficult to derive, and in many situations, it is required to artificially complete missing information, which is not present in the experimental data due to physical limitations of the experimental setting. Even if outside the scope of the current work, these briefly mentioned points are of highest importance and thus, they should not be underestimated.

To succinctly ponder on the computational efficiency that can be achieved by an optimal implementation of the approximate NLP, we can start by determining $\dim(\boldsymbol{x})$, the size of the vector of variables for the corresponding primal-dual formulation. Therefore, we have that:

- $\dim(\boldsymbol{q}) = \dim(\boldsymbol{\mu}) + \dim(\boldsymbol{\nu}) =$ number of nodes $\times$ number of nodal variables,
- $\dim(\boldsymbol{e}) = \dim(\boldsymbol{s}) = \dim(\boldsymbol{\lambda}) = \dim(\boldsymbol{\xi}) =$ number of elements $\times$ number of elemental variables $\times$ number of integration points,
- $\dim(\boldsymbol{x}) = 2\dim(\boldsymbol{q}) + 6\dim(\boldsymbol{e})$.

So $\dim(\boldsymbol{x}) = 2 \times$ number of nodes $\times$ number of nodal variables $+ 6 \times$ number of elements $\times$ number of elemental variables $\times$ number of integration points. It is assumed, that the kinematic constraints are enforced at the nodal level, and that the constitutive ones at the elemental level. Nonstandard finite element formulations that need non-integrable constraints in time and space, that is, vanishing shear for the Kirchhoff rods[26] or vanishing twist for the nonholonomic rotating rigid body,[27] would require further considerations. All involved matrices have a high degree of sparsity and thus, can be implemented taking advantage of this feature. Special attention has to be paid to the fact that nodal constraints, which are at most quadratic, and the null-space matrices, which are at most linear, can be computed analytically. This allows computing the null-space matrix for the whole system very efficiently and the subsequent elimination of multipliers from the balance equation can be computed by a sparse matrix-vector product. Such features are also present in the underlying finite element approximation (FEM), whose number of unknowns, after removing the Lagrange multipliers is equal to the number of nodes times the number of nodal variables. The elemental variables are obtained directly from the nodal variables, and thus, they do not increase the dimension of the residuum vector. With optimized implementations and under the assumption that as usual the computational effort of an iteration is dominated by solving, respectively, the Newton system (FEM) and the KKT system (approximate NLP), we can say that in general the effort for the approximate NLP approach is roughly the same as the effort for the FEM approach multiplied by a small constant factor. This is because the Newton system essentially comprises the constraints of the KKT system, except that the variables $(\check{\boldsymbol{e}}, \check{\boldsymbol{s}})$ and $(\boldsymbol{e}, \boldsymbol{s})$ are not distinguished. Thus, any extra effort in solving the KKT system is related to its upper left block, the Hessian matrix of the Lagrangian, since the symmetric block structure of the KKT matrix will be exploited. The exact value of the small constant factor then depends on the relative dimensions of the blocks and on their sparsity.

2.3 | Differences between the static and dynamic cases

There are important conceptual differences that need to be carefully analyzed when we formulate optimization problems corresponding to the static and dynamic cases. The static variant can be classified as an extension of the classical boundary value problem, cf. the standard mechanical setting. The constraint equation related to the balance equation results from

the direct spatial discretization of the weak form of the equilibrium statement. Therefore, the only choices that can be made are, in principle, the structural elements and the finite element technology to be used for investigating a particular kind of structure.

In contrast, the dynamic variant can be classified as an extension of the classical initial-boundary value problem, cf. the standard mechanical setting, and thus, a new dimension of complexity is to be considered. The restriction related to the equilibrium statement can be approximated for instance by the direct temporal discretization of the continuous balance equations as done by Kirchdoerfer and Ortiz,[11] who employed the Newmark method in an entropy maximizing context. But it can also be addressed by approximations inspired by discrete variational principles. These are, to the best of our knowledge, the only suitable structure-preserving approaches in Data-Driven Computational Mechanics since they do not require the existence of a potential energy function, which means that the discrete internal force and stiffness can be composed from the evaluation of the continuous terms. Such an approximation has profound consequences when we define the related nonlinear optimization problems. They should, by design, avoid destroying the order of the time integration scheme and preserve at the same time the motion-invariant properties, an aspect that plays no role in the static context.

As already introduced in the previous section, let us consider three successive equidistant time instants, that is, t_{i-1}, t_i, t_{i+1}, and two algorithmic intermediate time instants, that is, $t_{i-\frac{1}{2}}, t_{i+\frac{1}{2}}$. A correct definition of the nonlinear optimization problem for the dynamic case requires the cost function, the compatibility equation and the constitutive restriction to be evaluated at the time instant $t_{i+\frac{1}{2}}$. The kinematic restrictions are to be computed at the time instant t_{i+1}. Meanwhile, the dynamic equilibrium is to be evaluated at the time instant t_i, which requires information from the time instants $t_{i-1}, t_{i-\frac{1}{2}}, t_i, t_{i+\frac{1}{2}}, t_{i+1}$. This means that the nonlinear optimization problem for the static case cannot be recovered from the nonlinear optimization problem for the dynamic case. Moreover, as the restriction forces are evaluated at the time instant t_i and the kinematic restrictions are evaluated at the time instant t_{i+1}, there is no necessity for computing the derivatives of the null-space matrix for building the KKT matrix (because this is evaluated at the same instant as the restriction forces and not in the current configuration at time instant t_{i+1}). From the viewpoint of efficient numerical methods, this is of highest relevance, since the calculation of the null-space matrix involves the numerical decomposition of the Jacobian matrix of the constraints and thus, the derivative should be evaluated numerically, which is highly inefficient. This very favorable feature is not present in the static problem, which requires the calculation of the derivatives of the null-space matrix since the restriction forces are always evaluated at the current configuration. This fact has also some consequences on the necessary and sufficient optimality conditions. The dynamic solver needs an initialization step to correctly impose the initial conditions in terms of discrete momenta (see, for instance, the works on variational integration by Lew et al.[14,15]), which is achieved as a kinetic restriction and plays again no role for the static case. Additionally, the dynamic case provides a natural warm-start for the algorithm, which is another feature that is not present in the static solver, in which homotopy methods can be employed to this end. This missing feature may lead of course to convergence problems and could require the globalization of the optimization algorithm employed.

In summary, even provided that the static and dynamic cases can be formulated using the same optimization principles, the resulting nonlinear optimization problems are different and thus, not equivalent in any form. However, it is very appealing that several nonequivalent nonlinear optimization problems can be correctly derived by means of the same optimization principles. In this context, we consider that a principle is a guideline that is to be followed in order to derive the corresponding governing equations, namely, the KKT conditions for optimality. This is also what we would expect from a general framework such as the one we are proposing here.

3 | SPECIALIZATION OF THE PROPOSED APPROACH

In this section, we describe a structural model that is reformulated within the proposed setting of Data-Driven Computational Dynamics. The model is a Data-driven Geometrically Exact Beam that is given in a frame-invariant path-independent finite element formulation. It relies on a kinematically constrained approach, where the orientation of the cross section is described by means of three vectors that are constrained to be mutually orthonormal. This example has a very favorable mathematical structure that is exploited to derive analytically all the ingredients related to the finite element formalism.

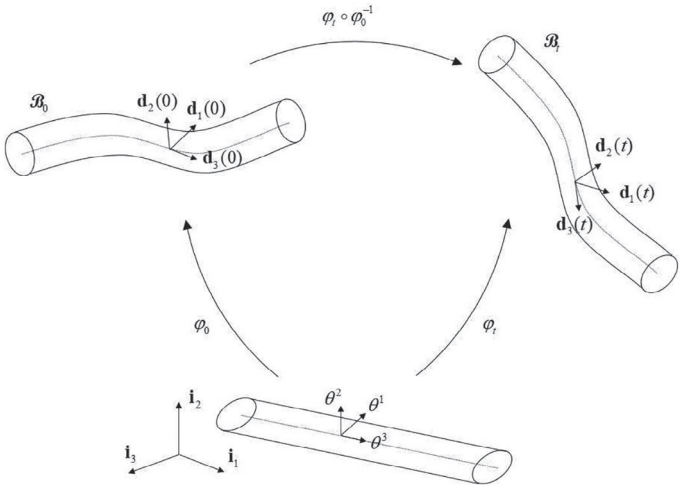

FIGURE 1 The geometrically exact beam: evolution among configurations through the regular motion $\boldsymbol{\varphi}(\cdot;t)\circ\boldsymbol{\varphi}(\cdot;0)^{-1}$

3.1 | Data-driven geometrically exact beam (dynamic setting)

The position of any point belonging to the beam shown in Figure 1 can be written as

$$\boldsymbol{\varphi}(\boldsymbol{\theta}) = \boldsymbol{\varphi}_0(\theta^3) + \theta^1\boldsymbol{d}_1(\theta^3) + \theta^2\boldsymbol{d}_2(\theta^3) \in \mathbb{R}^3, \tag{35}$$

in which $\boldsymbol{\varphi}_0 \in \mathbb{R}^3$ is the position vector of the beam axis and $\boldsymbol{d}_1 \in S^2$, $\boldsymbol{d}_2 \in S^2$ together with $\boldsymbol{d}_3 \in S^2$ are three mutually orthonormal directors. The directors can be described by means of the unit sphere, which is a nonlinear, smooth, compact, two-dimensional manifold that can be embedded in $\mathbb{R}^3$ as

$$S^2 := \{\boldsymbol{d} \in \mathbb{R}^3 | \boldsymbol{d}^T\boldsymbol{d} = 1\}. \tag{36}$$

Special attention must be paid to the fact that this manifold possesses no special algebraic structure, specifically group-like structure.[28] On that basis, the rotation tensor for the cross section is simply obtained as $\boldsymbol{\Lambda} = \boldsymbol{d}_1 \otimes \boldsymbol{i}^1 + \boldsymbol{d}_2 \otimes \boldsymbol{i}^2 + \boldsymbol{d}_3 \otimes \boldsymbol{i}^3 \in SO(3)$, in which $\{\boldsymbol{i}^1, \boldsymbol{i}^2, \boldsymbol{i}^3\}$ is the dual basis of the ambient space $\mathbb{E}^3$ ($\mathbb{R}^3$ with the standard Euclidean structure), that is, the basis of the space of row vectors. The group of rotations is a nonlinear, smooth, compact, three-dimensional manifold defined as

$$SO(3) := \{\boldsymbol{\Lambda} \in \mathbb{R}^{3\times3} | \boldsymbol{\Lambda}^T\boldsymbol{\Lambda} = \boldsymbol{I}, \det\boldsymbol{\Lambda} = 1\}. \tag{37}$$

In contrast to the unit sphere, this manifold does possess a group-like structure when considered with the tensor multiplication operation, hence it is a Lie group.

The set of parameters $\boldsymbol{\theta} = (\theta^1, \theta^2, \theta^3)$ is chosen in a way that the vector $\overline{\boldsymbol{\theta}} = \theta^1\boldsymbol{d}_1 + \theta^2\boldsymbol{d}_2$ completely describes the cross section. In the context of geometrically exact beams, the doubly covariant Green-Lagrange strain tensor, $\boldsymbol{E}_\flat(\boldsymbol{\varphi})$, can be simplified by eliminating quadratic strains. Thus, its components are approximated as

$$E_{ij} \approx \text{symm}(\delta_{i3}\delta_{jk}((\gamma^k - \gamma^k_{\text{ref}}) - \epsilon^k_{lm}\overline{\theta}^l(\omega^m - \omega^m_{\text{ref}}))), \tag{38}$$

where symm$(\cdot)$ stands for the symmetrization of the tensor considered. The subindex "ref" indicates the stress-free configuration, δ_{ij} denotes the Kronecker delta, and ϵ^i_{jk} is the alternating symbol that appears in the computation of the cross product in three-dimensional Euclidean space. From now on, we set $\theta^3 = \sigma$ to indicate every reference related to the arc length of the beam. The scalars γ^i are the components of a first deformation vector defined as

$$\boldsymbol{\gamma} = \begin{pmatrix} \boldsymbol{d}_1{}^T\partial_\sigma\boldsymbol{\varphi}_0 \\ \boldsymbol{d}_2{}^T\partial_\sigma\boldsymbol{\varphi}_0 \\ \boldsymbol{d}_3{}^T\partial_\sigma\boldsymbol{\varphi}_0 \end{pmatrix}. \tag{39}$$

For shear refer to first and second components, and for elongation refer to the third one. The scalars ω^i are the components of a second deformation vector defined as

$$\boldsymbol{\omega} = \frac{1}{2}\begin{pmatrix} \boldsymbol{d}_3{}^T\partial_\sigma \boldsymbol{d}_2 - \boldsymbol{d}_2{}^T\partial_\sigma \boldsymbol{d}_3 \\ \boldsymbol{d}_1{}^T\partial_\sigma \boldsymbol{d}_3 - \boldsymbol{d}_3{}^T\partial_\sigma \boldsymbol{d}_1 \\ \boldsymbol{d}_2{}^T\partial_\sigma \boldsymbol{d}_1 - \boldsymbol{d}_1{}^T\partial_\sigma \boldsymbol{d}_2 \end{pmatrix}. \tag{40}$$

For bending refer to first and second components, and for torsion refer to the third one. For sake of compactness, let us introduce the vector containing all kinematic fields,

$$\boldsymbol{q}(\sigma) = (\boldsymbol{\varphi}_0(\sigma)^T, \boldsymbol{d}_1(\sigma)^T, \boldsymbol{d}_2(\sigma)^T, \boldsymbol{d}_3(\sigma)^T)^T, \tag{41}$$

and the vector that gathers the two strain measures obtained from the kinematic field,

$$\boldsymbol{e}(\boldsymbol{q}) = \begin{pmatrix} \boldsymbol{\gamma}(\boldsymbol{q}) - \boldsymbol{\gamma}_{\text{ref}} \\ \boldsymbol{\omega}(\boldsymbol{q}) - \boldsymbol{\omega}_{\text{ref}} \end{pmatrix}. \tag{42}$$

Additionally, we need to introduce the vector containing all generalized "strain" fields that is going to be tied by the compatibility equation,

$$\boldsymbol{e} = \begin{pmatrix} \boldsymbol{\gamma} - \boldsymbol{\gamma}_{\text{ref}} \\ \boldsymbol{\omega} - \boldsymbol{\omega}_{\text{ref}} \end{pmatrix}, \tag{43}$$

and the vector containing the two generalized "stress" fields,

$$\boldsymbol{s} = \begin{pmatrix} \boldsymbol{n} \\ \boldsymbol{m} \end{pmatrix}, \tag{44}$$

which contains the cross sectional force and moment resultants, that is, three force components and three moment components.

The operator that relates the variation of the displacement-based strains to the variation of the kinematic fields through the relation $\delta\boldsymbol{e}(\boldsymbol{q}) = \mathfrak{B}(\boldsymbol{q})\delta\boldsymbol{q}$ has the explicit form

$$\mathfrak{B}(\boldsymbol{q}) = \frac{1}{2}\begin{bmatrix} 2\boldsymbol{d}_1{}^T\partial_\sigma & 2\partial_\sigma\boldsymbol{\varphi}_0{}^T & \boldsymbol{0} & \boldsymbol{0} \\ 2\boldsymbol{d}_2{}^T\partial_\sigma & \boldsymbol{0} & 2\partial_\sigma\boldsymbol{\varphi}_0{}^T & \boldsymbol{0} \\ 2\boldsymbol{d}_3{}^T\partial_\sigma & \boldsymbol{0} & \boldsymbol{0} & 2\partial_\sigma\boldsymbol{\varphi}_0{}^T \\ \boldsymbol{0} & \boldsymbol{0} & \boldsymbol{d}_3{}^T\partial_\sigma - \partial_\sigma\boldsymbol{d}_3{}^T & \partial_\sigma\boldsymbol{d}_2{}^T - \boldsymbol{d}_2{}^T\partial_\sigma \\ \boldsymbol{0} & \partial_\sigma\boldsymbol{d}_3{}^T - \boldsymbol{d}_3{}^T\partial_\sigma & \boldsymbol{0} & \boldsymbol{d}_1{}^T\partial_\sigma - \partial_\sigma\boldsymbol{d}_1{}^T \\ \boldsymbol{0} & \boldsymbol{d}_2{}^T\partial_\sigma - \partial_\sigma\boldsymbol{d}_2{}^T & \partial_\sigma\boldsymbol{d}_1{}^T - \boldsymbol{d}_1{}^T\partial_\sigma & \boldsymbol{0} \end{bmatrix}. \tag{45}$$

The mass matrix per unit of length is given by

$$\boldsymbol{M} = \begin{bmatrix} \mathscr{E}_{00}\boldsymbol{I} & \mathscr{E}_{01}\boldsymbol{I} & \mathscr{E}_{02}\boldsymbol{I} & \boldsymbol{0} \\ \mathscr{E}_{01}\boldsymbol{I} & \mathscr{E}_{11}\boldsymbol{I} & \mathscr{E}_{12}\boldsymbol{I} & \boldsymbol{0} \\ \mathscr{E}_{02}\boldsymbol{I} & \mathscr{E}_{12}\boldsymbol{I} & \mathscr{E}_{22}\boldsymbol{I} & \boldsymbol{0} \\ \boldsymbol{0} & \boldsymbol{0} & \boldsymbol{0} & \boldsymbol{0} \end{bmatrix}, \tag{46}$$

where $\boldsymbol{I}$ is the 3×3-identity matrix and $\mathscr{E}_{ij}$ is computed by means of $\int_{\mathcal{A}_0} \varrho_0 \theta^i \theta^j \mathrm{d}\mathcal{A}_0$ for i and j from 0 to 2, with ϱ_0 and $\mathcal{A}_0$ representing the mass density per unit volume and the cross sectional area, both at the reference configuration, correspondingly.

To perform the spatial discretization of the geometrically exact beam into two-node finite elements, we approximate the kinematic fields as well as their admissible variations with first-order Lagrangian functions. Upon such a discretization, we have that $\mathfrak{B} \rightsquigarrow \boldsymbol{B}$. The adopted numerical quadrature for the integration of elemental contributions is the standard Gauss-Legendre quadrature rule. As usual, the integrals involving internal terms are computed by means of a one-point integration scheme that avoids shear locking issues. Therefore, the evaluation of the kinematic fields at the single Gauss

point is in fact an average of the nodal values, and their derivatives with respect to the arc length turn out to be the simplest directed difference of the nodal values. Moreover, even for coarse discretizations, no additional residual stress corrections are necessary. For an extensive treatment of geometrically exact beams in the non-data-driven finite element setting, see References 29-33.

Finally and as in Reference 31, the mutual orthonormality condition among the directors is enforced at the nodal level by means of the internal constraint

$$\boldsymbol{g}(\boldsymbol{q}) = \frac{1}{2}\begin{pmatrix} \boldsymbol{d}_1 \cdot \boldsymbol{d}_1 - 1 \\ \boldsymbol{d}_2 \cdot \boldsymbol{d}_2 - 1 \\ \boldsymbol{d}_3 \cdot \boldsymbol{d}_3 - 1 \\ 2\boldsymbol{d}_2 \cdot \boldsymbol{d}_3 \\ 2\boldsymbol{d}_1 \cdot \boldsymbol{d}_3 \\ 2\boldsymbol{d}_1 \cdot \boldsymbol{d}_2 \end{pmatrix}. \tag{47}$$

The associated Jacobian matrix is

$$\boldsymbol{G}(\boldsymbol{q}) = \begin{bmatrix} \boldsymbol{0} & \boldsymbol{d}_1{}^T & \boldsymbol{0} & \boldsymbol{0} \\ \boldsymbol{0} & \boldsymbol{0} & \boldsymbol{d}_2{}^T & \boldsymbol{0} \\ \boldsymbol{0} & \boldsymbol{0} & \boldsymbol{0} & \boldsymbol{d}_3{}^T \\ \boldsymbol{0} & \boldsymbol{0} & \boldsymbol{d}_3{}^T & \boldsymbol{d}_2{}^T \\ \boldsymbol{0} & \boldsymbol{d}_3{}^T & \boldsymbol{0} & \boldsymbol{d}_1{}^T \\ \boldsymbol{0} & \boldsymbol{d}_2{}^T & \boldsymbol{d}_1{}^T & \boldsymbol{0} \end{bmatrix}. \tag{48}$$

The null-space projector corresponding to the internal constraint at the nodal level can be built by visual inspection of the Jacobian matrix as

$$\boldsymbol{N}(\boldsymbol{q}) = \begin{bmatrix} \boldsymbol{I} & \boldsymbol{0} & \boldsymbol{0} & \boldsymbol{0} \\ \boldsymbol{0} & \hat{\boldsymbol{d}}_1 & \hat{\boldsymbol{d}}_2 & \hat{\boldsymbol{d}}_3 \end{bmatrix}^T, \tag{49}$$

where the algebraic operator $\widehat{(\cdot)}$ emulates the cross product.

Since the formulation of constraints related to usual boundary conditions, for example, rigid support, simple support, movable support inter alia, are represented by linear equations in the nodal variables and thus, their treatment is straightforward, we omit their systematic presentation. For further details, see References 32,34.

Finally, having at hand all vectors and matrices indicated within this subsection, the construction of the equations corresponding to the optimality conditions and their derivatives is straightforward.

4 | NUMERICAL INVESTIGATIONS

In this section, we present three numerical examples that show the potential of the proposed approximate NLP for Data-Driven Computational Dynamics. Specifically, we consider its specialization to the geometrically exact beam model. The first example presents a verification of the proposed formulation, taking the underlying three-director based standard FE formulation for geometrically exact beams that is combined with an energy-momentum time integration scheme based on the "average vector field"[22] as proposed for slender structures in References 32,33. Such scheme preserves not only the linear momentum, angular momentum and total energy, but also the symmetry of the tangent stiffness matrix, a feature that is in general unavailable in energy-momentum approaches based on stress formulas by González,[21] Romero,[23] and Gebhardt et al.[33] We refer to that approach as EM-FEM. Such a reference numerical model is equipped with the simplest linear constitutive law. In the second example, we investigate the behavior of our framework for nonsymmetric explicitly-defined nonlinear constitutive laws, namely $\boldsymbol{s} = \boldsymbol{s}(\boldsymbol{e})$. Finally, we investigate in the third example the behavior of our framework for nonsymmetric implicitly-defined nonlinear constitutive laws, namely $\boldsymbol{e} = \boldsymbol{e}(\boldsymbol{s})$.

The problems considered along the first and second examples can also be addressed by any standard FE formulation in its dynamic setting. The problem considered along the third one can be easily addressed in the context of our approximate

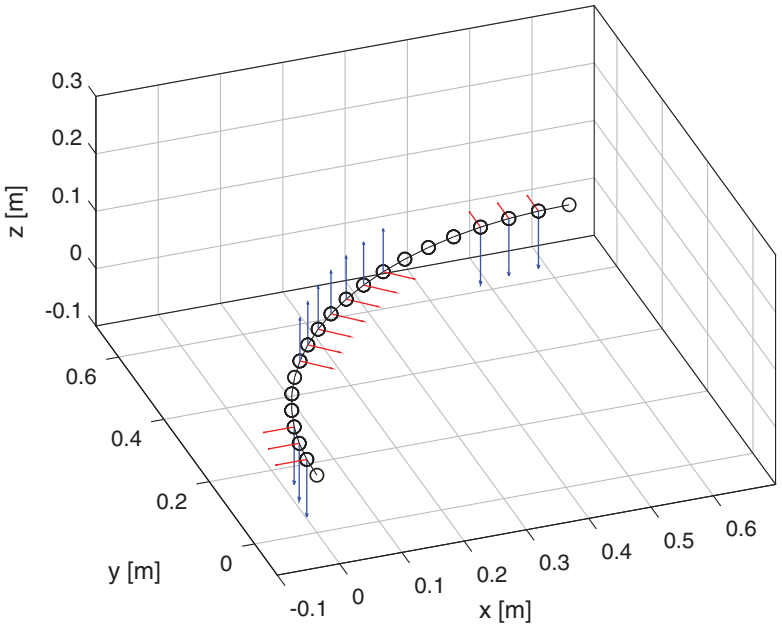

FIGURE 2 Finite element representation of the beam structure. Circles indicate nodes with internal constraints only. Blue and red arrows denote forces along the vertical direction z and in the horizontal x-y-plane, respectively

NLP approach, but not by standard FEM. Whether such a constitutive law is physically feasible or not will be considered in future works.

All the three examples are built on a curved beam structure whose geometry is described by a quarter of a circular arc with a total arc length of 1 m, which corresponds to a radius of $\frac{2}{\pi}$ m. The (nonphysical) inertial properties are $\mathscr{E}_{00} = 10$ kg/m and $\mathscr{E}_{11} = \mathscr{E}_{22} = 20$ kgm. The structure is uniformly discretized into 20 two-node finite elements (ie, a total of 21 nodes) and no further kinematic restrictions than the internal ones (orthonormality condition among the three directors) are enforced. Figure 2 shows the finite element representation and loads applied. The first node is located at the position $(0, 0, 0)$ m. The nodes 2 to 4 are loaded with vertical nodal forces $(0, 0, -20)$ N and horizontal nodal forces $(-10, 0, 0)$ N. For the nodes 8 to 14, we have $(0, 0, 15)$ N and $(7.5, -7.5, 0)$ N. For the nodes 18 to 20, we have $(0, 0, -20)$ N and $(0, 10, 0)$ N. This setting has been chosen because the action of combined spatial loads creates complex strain-stress states in space and time. Finally, the loads are multiplied with a function that describes the variation of the external forces over time, which is defined by (50), that is, $\boldsymbol{f}^{\text{ext}} = a(t)(f_1\boldsymbol{i}^1 + f_2\boldsymbol{i}^2 + f_3\boldsymbol{i}^3)$. For all numerical examples, the relative error-based tolerance of 10^{-12} has been set for the Newton iteration.

$$a(t) = \begin{cases} 2t & \text{for } 0 \leq t < 0.5 \\ 2 - 2t & \text{for } 0.5 \leq t < 1 \\ 0 & \text{for } t \geq 1 \end{cases}. \tag{50}$$

As far as we know, our previous article[10] is the only work in the context of Data-Driven Computational Mechanics that handles geometrically exact beams. It considers, however, only the static case. Handling kinematic constrains to implicitly define the group of rotations $SO(3)$ needs to be complemented by the null-space method, through which repeated multipliers that would otherwise cause singular KKT matrices are eliminated. The application of the null-space method differs notably from the static case as explained previously. The behavior of geometrically exact beams in general elasticity has been studied to some extent, mostly subordinate to the existence of a hyperelastic potential. Further investigations in a dynamic context remain currently open. In synthesis, the geometrically exact beam presented here makes full use of the derived mathematical machinery and is thus complex enough from the mathematical point of view to test our proposed framework. Our target is to probe the concept, and thus, the simulation cases were selected to produce intuitive responses and exhibit similar complexity as other standard simulation cases considering the setting provided by Data-Driven Computational Mechanics, that is, truss and volume elements. In this initial stage that concerns the development of strategies at the root of the methods, we avoid counter-intuitive examples.

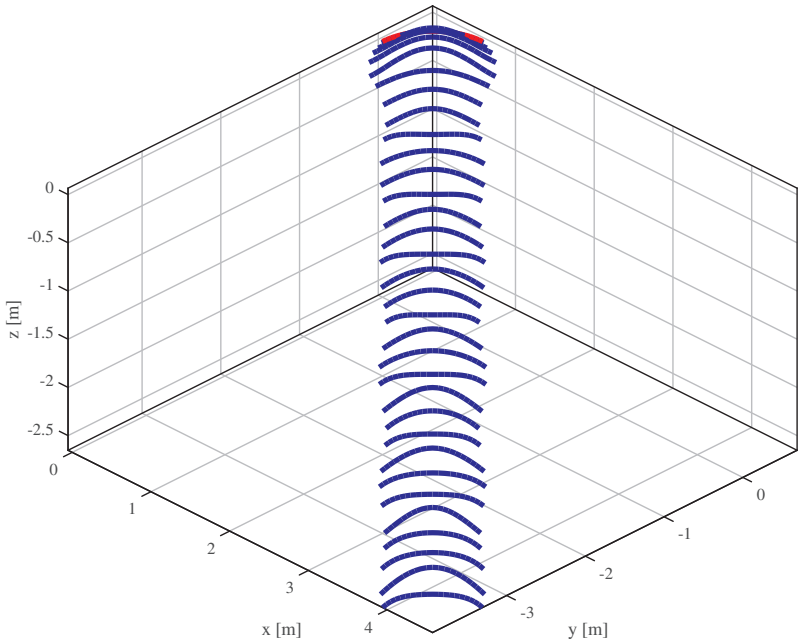

FIGURE 3 Verification (first example)—sequence of motion [Colour figure can be viewed at wileyonlinelibrary.com]

4.1 | Verification

As indicated, we first consider the beam structure described above and the simplest linear constitutive law, defined as

$$(\boldsymbol{g}^{\sharp}(\check{\boldsymbol{e}}_{i+\frac{1}{2}}, \check{\boldsymbol{s}}_{i+\frac{1}{2}}))^{i} = \check{s}^{i} - a^{ii}\check{e}_{i} = 0 \qquad \text{or alternatively as} \qquad (\boldsymbol{g}_{\flat}(\check{\boldsymbol{e}}_{i+\frac{1}{2}}, \check{\boldsymbol{s}}_{i+\frac{1}{2}}))_{i} = \check{e}_{i} - a_{ii}\check{s}^{i} = 0, \tag{51}$$

with $a^{ii} = a_{ii}^{-1}$ and the (nonphysical) values $a^{11} = a^{22} = 75\,\text{N}$, $a^{33} = 100\,\text{N}$, $a^{44} = a^{55} = 100\,Nm^2$ and $a^{66} = 200\,Nm^2$. The weight matrix $\boldsymbol{C}$ is defined as the identity.

Figure 3 shows a sequence of motion, where the initial configuration plotted in red is located at the topmost position. It is possible to observe that the structure undergoes large displacements and large changes of curvature. However, as the geometry of the structure and applied loads are symmetric, and the constitutive law considered is antisymmetric, the response computed is perfectly symmetric as expected. By starting each subsequent optimization problem warmly, that is, taking as initial guess the converged solution of the previous optimization problem, the approximate NLP solver requires three iterations on average to find the solution. Meanwhile, the EM-FEM solver requires four iterations on average. The adopted EM-FEM warrants the discrete time invariance as well as the symmetry of the tangent stiffness matrix and thus, is a little bit harder to solve when compared to variational integrators, which do not render in general the discrete time invariance, see, for instance, Reference 15. In spite of the additional iteration, the EM-FEM is always faster in runtime than the approximate NLP solver. By considering the same mesh, the number of unknowns is smaller for the EM-FEM and in addition, such an approach is already highly optimized from the implementation point of view. Meanwhile, the implementation of the approximate NLP has not been yet been fully optimized. Table 1 presents the displacement and directors of the 11th node at $t = 4$ seconds for both formulations, namely results corresponding to the EM-FEM versus those corresponding to the approximate NLP. Table 2 shows comparatively the stationary values for the linear and angular momenta. Both tables demonstrate that the results obtained with the approximate NLP are in excellent agreement with the results obtained with the EM-FEM. Figures 4 and 5 present several time histories for the time interval $[0, 4]$ seconds: components of the cross sectional resultant force per unit length at the eighth element, components of the cross sectional resultant moment per unit length at the eighth element, components of the linear momentum, and components of the angular momentum. After an initial transient due to the presence of time varying loads, the resultant forces appear to reach a sort of oscillatory steady state. A similar observation can be made for the resultant moments. The linear and angular momenta reach, after the initial transient, stationary values that are identically preserved along the remainder of the simulation.

TABLE 1 Verification (first example)—nodal variables of the 11th node at $t = 4$ s; EM-FEM (top) vs approximate NLP (bottom)

comp.	φ_0 (m)	d_1 (-)	d_2 (-)	d_3 (-)
x	4.11665929	0.40215049	0.58161351	0.70711267
y	−3.48003891	−0.40215496	−0.58161692	0.70710732
z	−2.63091834	0.82252438	−0.56873242	0.00000122
x	4.11667597	0.40214954	0.58161417	0.70711267
y	−3.48005560	−0.40215401	−0.58161758	0.70710733
z	−2.63093328	0.82252532	−0.56873108	0.00000123

TABLE 2 Verification (first example)—linear and angular momenta; stationary values

comp.	l (EM-FEM) (Kgm/s)	l (approx. NLP) (Kgm/s)	j (EM-FEM) (Kgm²/s)	j (approx. NLP) (Kgm²/s)
x	11.25000000	11.25000000	1.39916065	1.39915722
y	11.25000000	11.25000000	6.17378053	6.17377710
z	−7.50000000	−7.50000000	−7.16199129	−7.16199130

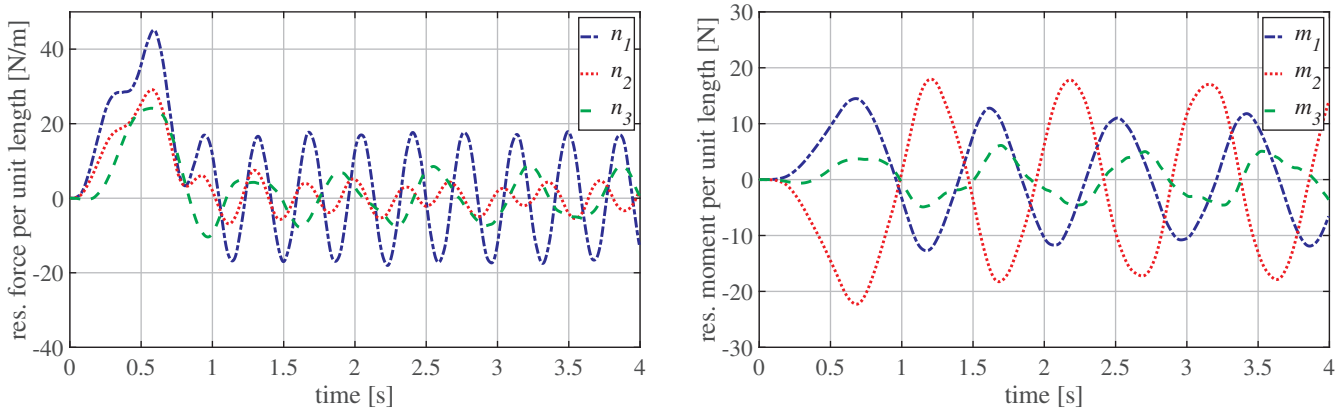

FIGURE 4 Verification (first example)—resultant force per unit length at the eighth element vs time (left), resultant moment per unit length at the eighth element vs time (right) [Colour figure can be viewed at wileyonlinelibrary.com]

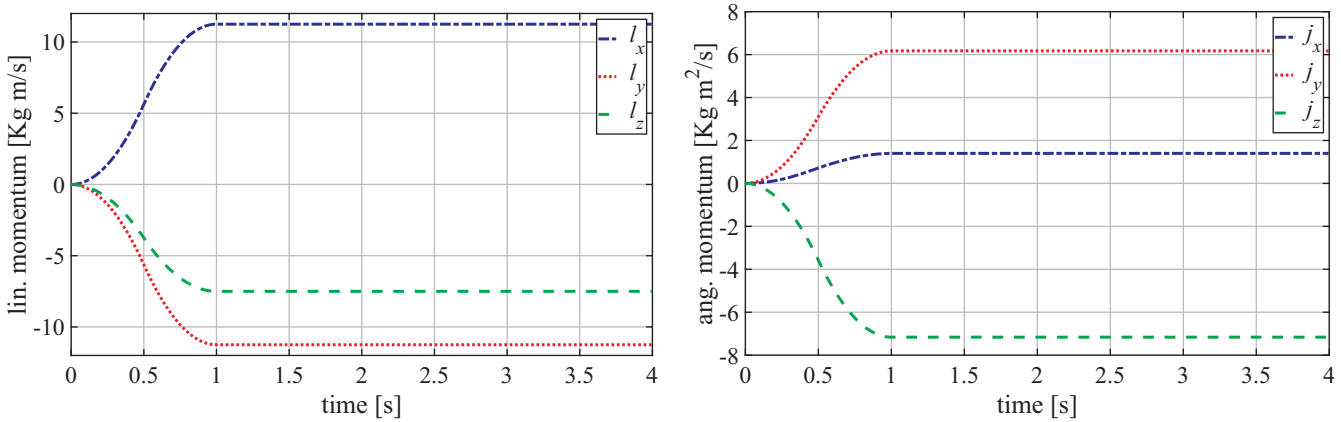

FIGURE 5 Verification (first example)—linear momentum vs time (left), angular momentum vs time (right) [Colour figure can be viewed at wileyonlinelibrary.com]

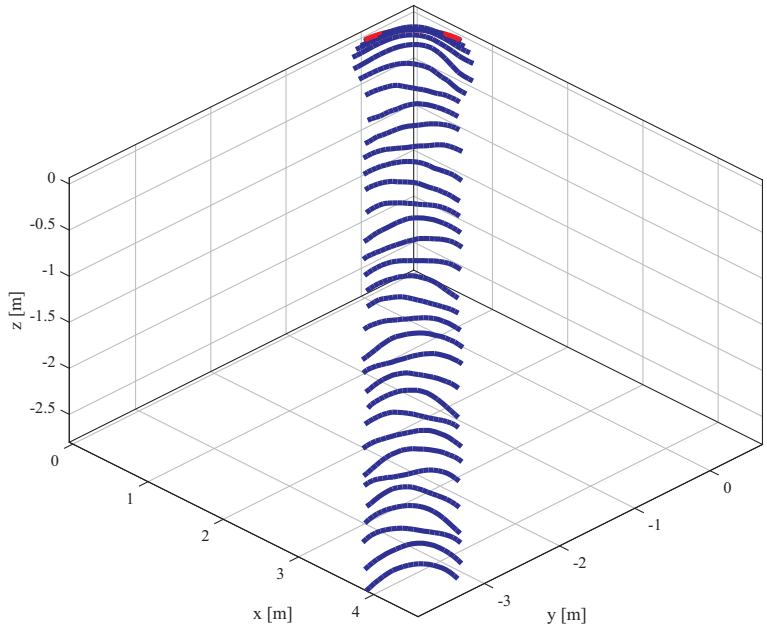

FIGURE 6 Explicit stress definition (second example)—sequence of motion [Colour figure can be viewed at wileyonlinelibrary.com]

comp.	l (approx. NLP) (Kgm/s)	j (approx. NLP) (Kgm^2/s)
x	11.25000000	2.18791717
y	11.25000000	5.90091563
z	−7.50000000	−7.37292831

TABLE 3 Explicit stress definition (second example)—linear and angular momenta; stationary values

4.2 | Explicit stress definition

In this second numerical example, we consider a nonlinear constitutive law given by

$$(\boldsymbol{g}^{\sharp}(\check{\boldsymbol{e}}_{i+\frac{1}{2}}, \check{\boldsymbol{s}}_{i+\frac{1}{2}}))^i = \check{s}^i - a^{ii}\check{e}_i - \frac{b^{iii}}{2}(\check{e}_i)^2, \tag{52}$$

where the stress resultants are defined *explicitly* in terms of the strain measures. For the coefficients a^{ii}, we use the same (nonphysical) values as in the verification example, and in addition, we set $b^{iii} = 0.6375a^{ii}$.

Figure 6 shows a sequence of motion, in which we observe that the structure undergoes large displacements and large changes of curvature. Even, provided that the geometry of the structure and applied loads are symmetric, the response computed is, as expected due to the nonsymmetric constitutive law considered, nonsymmetric. Figures 7 and 8 present, as in the previous example, several time histories. After an initial transient due to the presence of time varying loads, the resultant forces appear to reach no steady state and show some high-frequency content. A similar comment can be made for the resultant moments. However, no high-frequency content is to be distinguished. As before, the linear and angular momenta reach, after the initial transient, stationary values that are identically preserved. Table 3 presents the stationary values for the momenta. As a final comment, we can say that the approximate NLP requires normally three iterations to converge, when warmly started.

4.3 | Implicit stress definition

In this third numerical example, we consider a nonlinear constitutive law given by

$$(\boldsymbol{g}_{\flat}(\check{\boldsymbol{e}}_{i+\frac{1}{2}}, \check{\boldsymbol{s}}_{i+\frac{1}{2}}))_i = \check{e}_i - a_{ii}\check{s}^i - \frac{b_{iii}}{2}(\check{s}^i)^2, \tag{53}$$

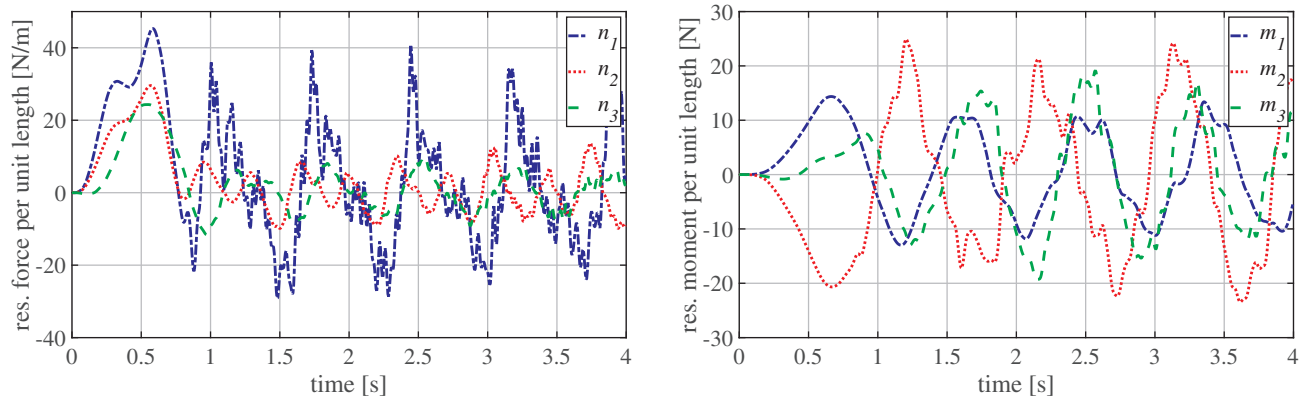

FIGURE 7 Explicit stress definition (second example)—resultant force per unit length at the eighth element vs time (left), resultant moment per unit length at the eighth element vs time (right) [Colour figure can be viewed at wileyonlinelibrary.com]

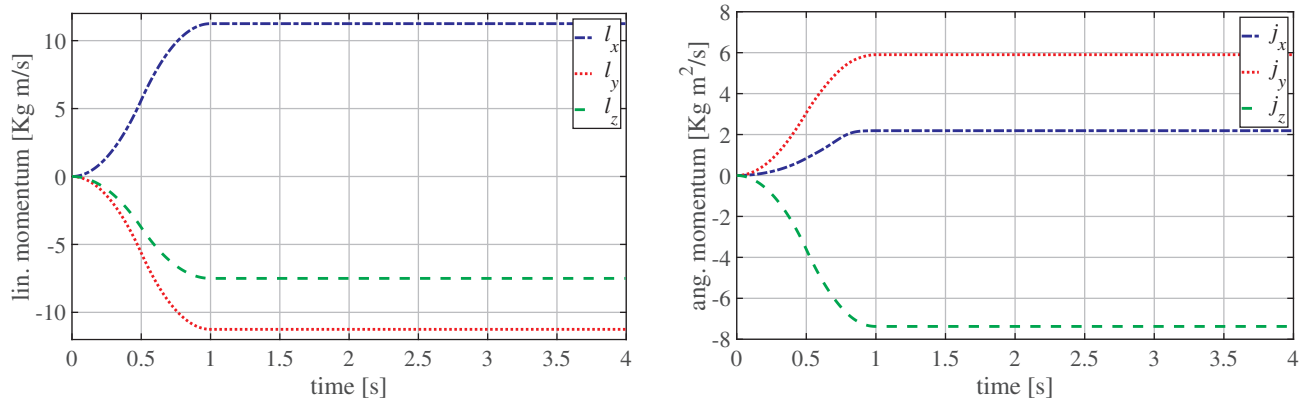

FIGURE 8 Explicit stress definition (second example)—linear momentum vs time (left), angular momentum vs time (right) [Colour figure can be viewed at wileyonlinelibrary.com]

where the stress resultants are defined *implicitly* in terms of the strain measures. For the coefficients a_{ii}, we consider the same (nonphysical) values as in the verification example, and in addition we set $b_{iii} = 0.015a_{ii}$.

Figure 9 presents a sequence of motion, in which we observe that the structure is undergoing large displacements and large changes of curvature. As in the previous case, the response is nonsymmetric due to the nonsymmetry of the constitutive law employed. Figures 10 and 11 show several time histories for the same variables that were showed in the two previous cases. After an initial transient due to the presence of time varying loads, the resultant forces do not appear to reach a steady state, and in contrast to the previous case, they show no high-frequency content. A similar observation can be made for the resultant moments, although some high-frequency content is evident. The linear and angular momenta reach, as expected, stationary values that are preserved along the simulation. Finally, Table 4 presents the stationary values for the momenta. Once again, the convergence properties are excellent as before.

5 | CONCLUDING REMARKS

In this article, we proposed an approximate nonlinear optimization problem for Data-Driven Structural Dynamics that extends the approach recently proposed by the authors in a purely static context.[10] In the dynamic setting, the resulting new formulation inherits the ability of handling: (i) kinematic constraints; and, (ii) materials whose stress-strain relationship can be implicitly approximated. Thus, the method is not limited by the requirement of some special functional structure for the definition of the material law. As the chosen dynamic setting is that inspired by a class of structure-preserving variational integrators, it cannot be reverted to the static approach developed previously, and therefore,

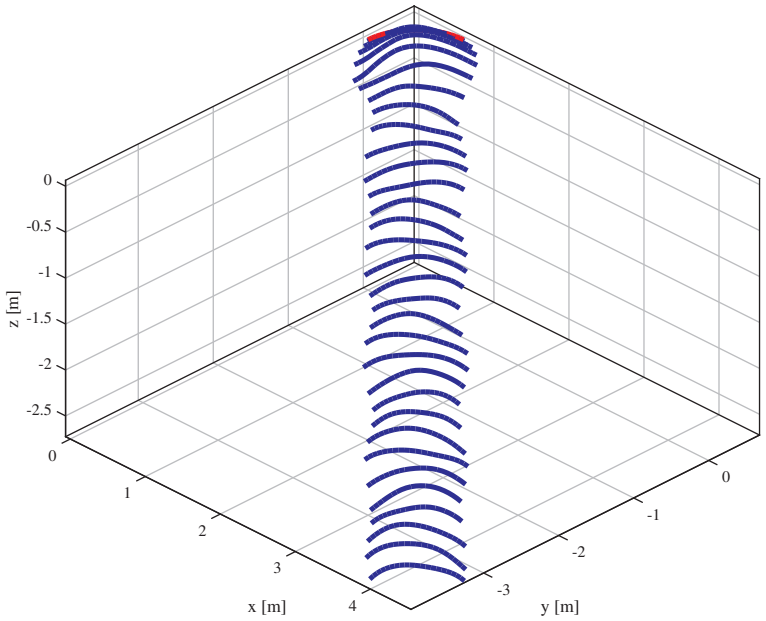

FIGURE 9 Implicit stress definition (third example)—sequence of motion [Colour figure can be viewed at wileyonlinelibrary.com]

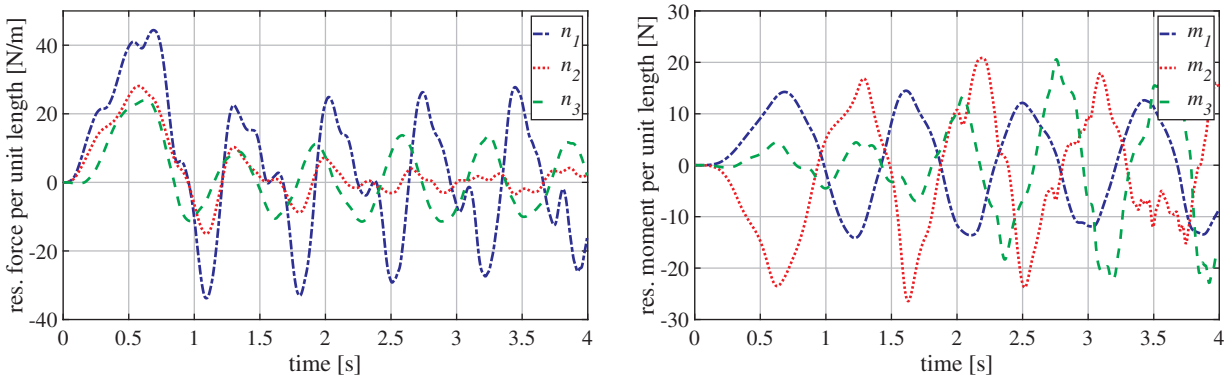

FIGURE 10 Implicit stress definition (third example)—resultant force per unit length at the eighth element vs time (left), resultant moment per unit length at the eighth element vs time (right) [Colour figure can be viewed at wileyonlinelibrary.com]

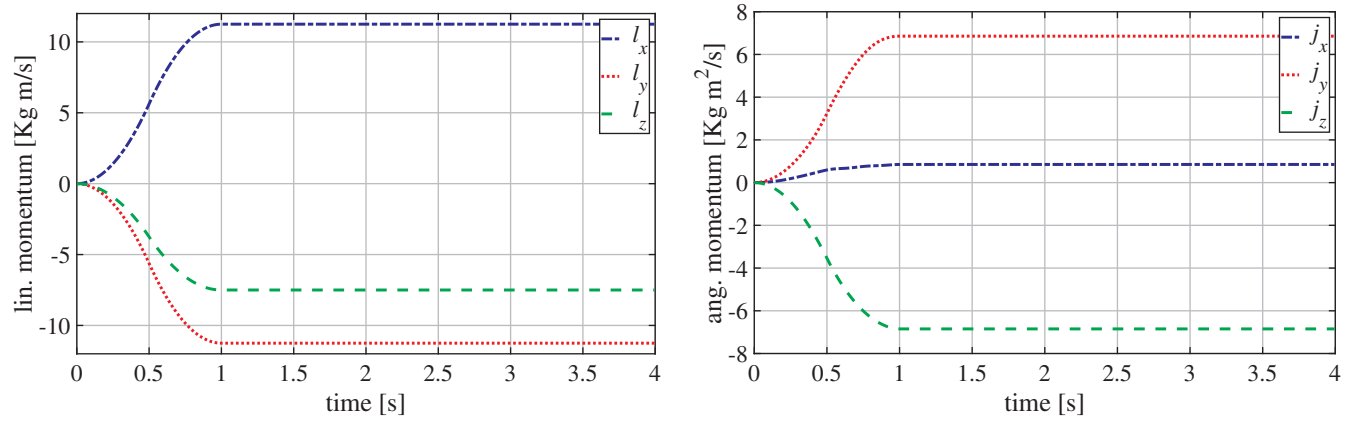

FIGURE 11 Implicit stress definition (third example)—linear momentum vs time (left), angular momentum vs time (right) [Colour figure can be viewed at wileyonlinelibrary.com]

TABLE 4 Implicit stress definition (third example)—linear and angular momenta; stationary values

comp.	l (approx. NLP) (Kgm/s)	j (approx. NLP) (Kgm^2/s)
x	11.25000000	0.85015476
y	11.25000000	6.85601926
z	−7.50000000	−6.84807263

it describes a different mathematical problem. For cases without external loads, however, the method preserves linear and angular momenta and for explicitly defined constitutive laws, it could be reverted to the discrete variational approach that preserves the underlying symplectic form. This aspect represents one main innovation of the current method.

The mathematical framework for Data-Driven Structural Dynamics was derived in detail and formulated in a self-contained fashion. To showcase the well-behaved properties of our approach, we specialized the method to the case of a geometrically exact beam formulation. We would like to emphasize that the extension of the Data-Driven Structural Dynamics paradigm to geometrically exact beam elements is another main innovation of the current work. For the numerical examples considered in this work, the convergence behavior was observed to be excellent. Moreover, our dynamic approach fully inherits the robustness, efficiency, and versatility properties of its static counterpart.

The results of the presented numerical examples clearly demonstrated that the proposed method represents a solid basis for further research. Possible research targets are the specialization to other structural models, for example, shells and solids, the extension to solving dynamic problems in multiple time scales, the inclusion of nonlinear optimization algorithms that can deal with inequalities and globalization techniques to warrant global convergence properties, inter alia.

ACKNOWLEDGMENTS

C. G. Gebhardt and R. Rolfes gratefully acknowledge the financial support of the Lower Saxony Ministry of Science and Culture (research project *ventus efficiens*, FKZ ZN3024) and the German Research Foundation (research project ENERGIZE, GE 2773/3-1 – RO 706/20-1) that enabled this work. D. Schillinger acknowledges support from the German Research Foundation through the DFG Emmy Noether Award SCH 1249/2-1, and from the European Research Council via the ERC Starting Grant "ImageToSim" (Action No. 759001). Open Access funding enabled and organized by Projekt DEAL.

CONFLICT OF INTEREST

The authors declare no conflict of interest.

ORCID

Cristian Guillermo Gebhardt https://orcid.org/0000-0003-0942-5526

REFERENCES

1. Kirchdoerfer T, Ortiz M. Data-driven computational mechanics. *Comput Methods Appl Mech Eng*. 2016;304:81-101. https://doi.org/10.1016/j.cma.2016.02.001.
2. Kirchdoerfer T, Ortiz M. Data driven computing with noisy material data sets. *Comput Methods Appl Mech Eng*. 2017;326:622-641. https://doi.org/10.1016/j.cma.2017.07.039.
3. Nguyen L, Keip M-A. A data-driven approach to nonlinear elasticity. *Comput Struct*. 2018;194:97-115. https://doi.org/10.1016/j.compstruc.2017.07.031.
4. Conti S, Müller S, Ortiz M. Data-driven problems in elasticity. *Arch Ration Mech Anal*. 2018;229:79-123. https://doi.org/10.1007/s00205-017-1214-0.
5. Eggersmann R, Kirchdoerfer T, Reese S, Stainer L, Ortiz M. Model-free data-driven inelasticity. *Comput Methods Appl Mech Eng*. 2019;350:81-99. https://doi.org/10.1016/j.cma.2019.02.016.
6. Kanno Y. Mixed-integer programming formulation of a data-driven solver in computational elasticity. *Optim Lett*. 2019;13:1505-1514. https://doi.org/10.1007/s11590-019-01409-w.
7. Ibañez R, Borzacchiello D, Aguado JV, et al. Data-driven non-linear elasticity: constitutive manifold construction and problem discretization. *Comput Mech*. 2017;60:813-826. https://doi.org/10.1007/s00466-017-1440-1.
8. Ibañez R, Abisset-Chavanne E, Aguado JV, González D, Cueto E, Chinesta F. A manifold learning approach to data-driven computational elasticity and inelasticity. *Archiv Comput Methods Eng*. 2018;25:47-57. https://doi.org/10.1007/s11831-016-9197-9.
9. Ibañez R, Abisset-Chavanne E, González D, Duval J-L, Cueto E, Chinesta F. Hybrid constitutive modeling: data-driven learning of corrections to plasticity models. *Int J Mater Form*. 2019;12:717-725. https://doi.org/10.1007/s12289-018-1448-x.

10. Gebhardt CG, Schillinger D, Steinbach MC, Rolfes R. A framework for data-driven structural analysis in general elasticity based on nonlinear optimization: the static case. *Comput Methods Appl Mech Eng*. 2020;365:112993. https://doi.org/10.1016/j.cma.2020.112993.
11. Kirchdoerfer T, Ortiz M. Data-driven computational dynamics. *Int J Numer Methods Eng*. 2018;113:1697-1710. https://doi.org/10.1002/nme.5716.
12. González F, Cueto E. Thermodynamically consistent data-driven computational mechanics. *Contin Mech Thermodyn*. 2019;31:239-253. https://doi.org/10.1007/s00161-018-0677-z.
13. Marsden JE, West M. Discrete mechanics and variational integrators. *Acta Numerica*. 2001;10:357-514. https://doi.org/10.1017/S096249290100006X.
14. Lew A, Marsden JE, Ortiz M, West M. Asynchronous variational integrators. *Arch Ration Mech Anal*. 2003;167:85-146. https://doi.org/10.1007/s00205-002-0212-y.
15. Lew A, Marsden JE, Ortiz M, West M. Variational time integrators. *Int J Numer Methods Eng*. 2004;60:153-212. https://doi.org/10.1002/nme.958.
16. Kale KG, Lew AJ. Parallel asynchronous variational integrators. *Int J Numer Methods Eng*. 2007;70:291-321. https://doi.org/10.1002/nme.1880.
17. Fong W, Darve E, Lew A. Stability of asynchronous variational integrators. *J Comput Phys*. 2008;227:8367-8394. https://doi.org/10.1016/j.jcp.2008.05.017.
18. Leyendecker S, Marsden JE, Ortiz M. Variational integrators for constrained dynamical systems. *Z Angew Math Mech*. 2008;88:677-708. https://doi.org/10.1002/zamm.200700173.
19. Betsch P, Hesch C, Sänger N, Uhlar S. Variational integrators and energy-momentum schemes for flexible multibody dynamics. *J Comput Nonlinear Dyn*. 2010;5:031001. https://doi.org/10.1115/1.4001388.
20. Lew AJ, Mata AP. A brief introduction to variational integrators. *CISM Int Centre Mech Sci Cours Lect*. 2016;565:201-291. https://doi.org/10.1007/978-3-319-31879-0_5.
21. Gonzalez O. Time integration and discrete Hamiltonian systems. *J Nonlinear Sci*. 1996;6:449-467. https://doi.org/10.1007/BF02440162.
22. McLachlan RI, Quispel GRW, Robideux N. Geometric integration using discrete gradients. *Philos Transact A Math Phys Eng Sci*. 1999;357:1021-1045. https://doi.org/10.1098/rsta.1999.0363.
23. Romero I. An analysis of the stress formula for energy-momentum methods in nonlinear elastodynamics. *Comput Mech*. 2012;50:603-610. https://doi.org/10.1007/s00466-012-0693-y.
24. Gebhardt CG, Romero I, Rolfes R. A new conservative/dissipative time integration scheme for nonlinear mechanical systems. *Comput Mech*. 2020;65:405-427. https://doi.org/10.1007/s00466-019-01775-3.
25. Crespo J, Latorre M, Montáns FJ. WYPIWYG hyperelasticity for isotropic, compressible materials. *Comput Mech*. 2017;59:73-92. https://doi.org/10.1007/s00466-016-1335-6.
26. Romero I, Gebhardt CG. Variational principles for nonlinear Kirchhoff rods. *Acta Mech*. 2020;231:625-647. https://doi.org/10.1007/s00707-019-02562-0.
27. Gebhardt C. G., Romero I. The rotating rigid body model based on a non-twisting frame; 2019. arXiv:1911.03666 [physics.class-ph]. https://arxiv.org/abs/1911.03666.
28. Eisenberg M, Guy R. A proof of the hairy ball theorem. *Am Math Mon*. 1979;86:571-574. https://doi.org/10.2307/2320587.
29. Romero I, Armero F. An objective finite element approximation of the kinematics of geometrically exact rods and its use in the formulation of an energy-momentum conserving scheme in dynamics. *Int J Numer Methods Eng*. 2002;54:1683-1716. https://doi.org/10.1002/nme.486.
30. Romero I. The interpolation of rotations and its application to finite element models of geometrically exact rods. *Comput Mech*. 2004;34:121-133. https://doi.org/10.1007/s00466-004-0559-z.
31. Betsch P, Steinmann P. Frame-indifferent beam finite elements based upon the geometrically exact beam theory. *Int J Numer Methods Eng*. 2001;54:1775-1788. https://doi.org/10.1002/nme.487.
32. Gebhardt CG, Hofmeister B, Hente C, Rolfes R. Nonlinear dynamics of slender structures: a new object-oriented framework. *Comput Mech*. 2019;63:219-252. https://doi.org/10.1007/s00466-018-1592-7.
33. Gebhardt CG, Steinbach MC, Rolfes R. Understanding the nonlinear dynamics of beam structures: a principal geodesic analysis approach. *Thin-Walled Struct*. 2019;140:357-362. https://doi.org/10.1016/j.tws.2019.03.009.
34. Hente C, Gebhardt CG, Pache D, Rolfes R. On the modal analysis of nonlinear beam and shell structures with singular mass and stiffness matrices. *Thin-Walled Struct*. 2019;144:106310. https://doi.org/10.1016/j.tws.2019.106310.

SUPPORTING INFORMATION

Additional supporting information may be found online in the Supporting Information section at the end of this article.

How to cite this article: Gebhardt C, Steinbach M, Schillinger D, Rolfes R. A framework for data-driven structural analysis in general elasticity based on nonlinear optimization: The dynamic case. *Int J Numer Methods Eng*. 2020;121:5447–5468. https://doi.org/10.1002/nme.6389